TU DELFT
Faculty of Mechanical, Maritime, and Materials Engineering

MASTER OF SCIENCE THESIS

Evaluation of Musculoskeletal Model Personalization for Gait Analysis of Children with Cerebral Palsy

Prepared by
Marcin Burdzy (4504585)
August 11, 2017

Project Supervisors:
Thomas Geijtenbeek – Technische Universiteit Delft
Marjolein van der Krogt – Vrije Universiteit Medisch Centrum

Table of Contents

ABSTRACT

Musculoskeletal modeling and simulation has become a prominent tool in clinical gait analysis with the ability to provide insight into the underlying mechanisms of human movement. However, generic cadaver-based models have been shown to poorly reflect live subjects, especially those with pathologies such as cerebral palsy (CP). The main purpose of this thesis was to evaluate the effect of model personalization on gait simulation outcomes between models of varying level of personalization. Gait data from 7 children with CP was used for simulations in OpenSim using 3 different model types for each: scaled generic (GS), scaled generic with tibial torsion and femoral anteversion (TTAF), and MRI-based. MRI-based model outcomes saw the greatest differences from GS models in the hip and upper leg, specifically hamstrings and quadriceps, but also experienced moderate differences in the lower leg. Similar results were found when comparing MRI to TTAF models. TTAF models differed from the GS models around the subtalar joint, mainly the tibialis anterior. Larger differences in kinematics, kinetics, and muscle activations were accompanied by changes to the most influential model parameters, in descending order of importance, these were: tendon slack length, moment arm length, and normalized muscle fiber length. Despite the differences between these models, there was no indication that either is more accurate or more suitable for clinical use.

1.0 Introduction

Gait analysis is the assessment of human locomotion through measurement of kinematics, kinetics, muscle activities, and spatio-temporal parameters throughout a stride. Figure 1 depicts a typical stride which consists of a sequence of motions that can be broken down into several phases, beginning with initial contact of the foot, then accepting, stabilizing and propelling the body mass forward, and finally preparing for the following step. While gait patterns among healthy people are fairly symmetrical and consistent, slight variations do exist due to differences in age, sex, size, and walking speed [1]. In a clinical setting, gait analysis is used to identify poor posture, injury, or pathology through larger abnormalities found in the gait pattern of a patient. In recent years, mathematical models and computer simulations have emerged as potential tools to aid in gait analysis by generating objective results, allowing “what if?” studies, and providing insight into how various musculoskeletal structures interact during movement [2].

Periods	Stance Period					Swing Period		
Tasks	Weight Acceptance		Single Limb Support		Swing Limb Advancement			
Phases	Initial Contact (0%)	Loading Response (0-10%)	Mid Stance (10-30%)	Terminal Stance (30-50%)	Pre Swing (50-60%)	Initial Swing (60-75%)	Mid Swing (75%-87%)	Terminal Swing (87-100%)
Critical Events	• Heel first initial contact	• Hip stability • Controlled knee flexion for shock absorption • Controlled ankle PF	• Controlled tibial advancement	• Controlled ankle DF with heel rise • Trailing limb posture	• Passive knee flexion to 40° • Rapid ankle PF	• Max knee flexion (>60°)	• Max hip flexion (30°) • DF to neutral	• Knee extension to neutral

Figure 1: Normalized gait stride [3]

Musculoskeletal Models and Personalization

Musculoskseletal (MS) models are simplified mathematical representations of the human body focused on movement generation. Software packages centered on MS modeling and simulations have been developed for scientific use. The research in this paper uses OpenSim 3.3 [4], which is freely available online and includes pre-made models such as the Gait 2392 lower extremity model. Hill-Type muscle models are widely used as the force-generating components of these MS models, combining 3 main elements to represent a complete muscle-tendon unit (MTU) as illustrated in Figure 2. These elements are:

i. Contractile Element (CE) – force-length-velocity relationship of the muscle fiber’s sarcomere
ii. Passive Element (PE) – viscoelastic properties of connective tissue; in parallel with the CE
iii. Series Element (SE) – viscoelastic properties of the tendon aponeuroses; in series with CE

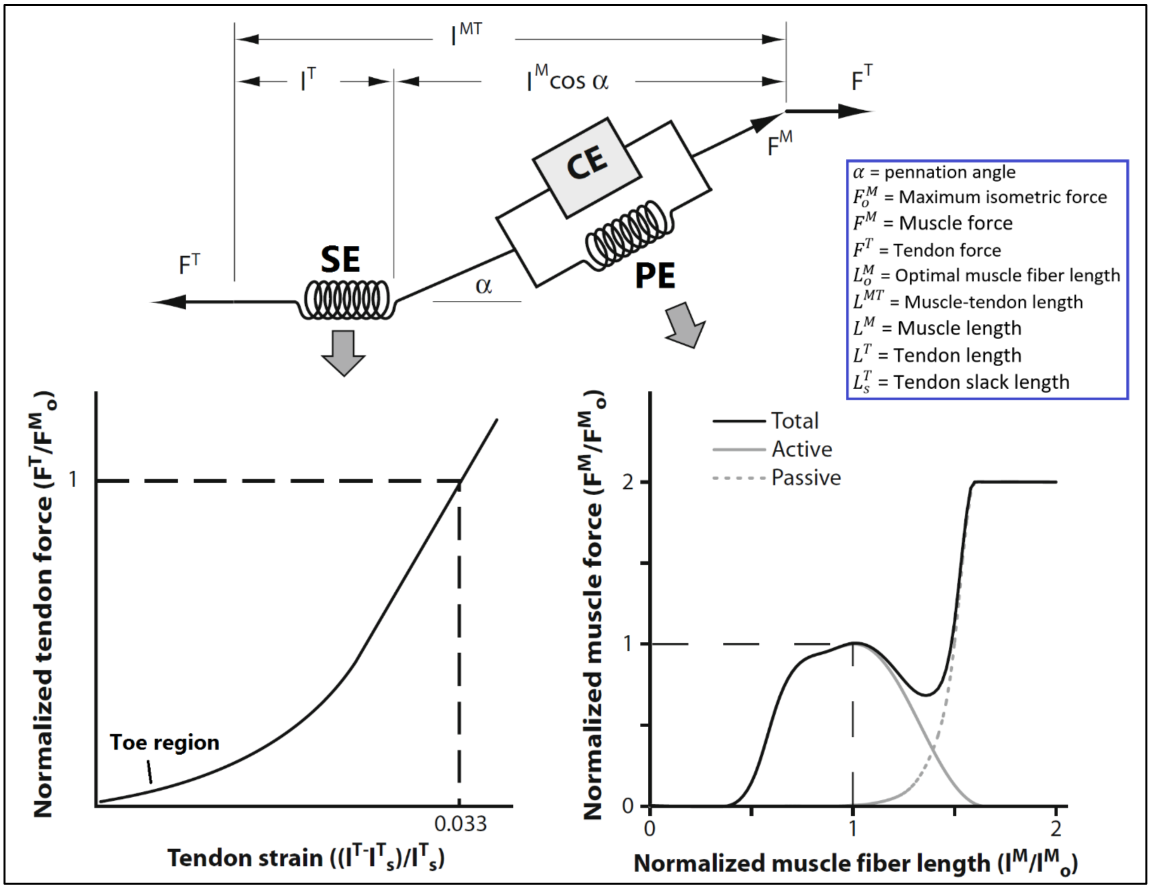

Figure 2: Hill-Type Muscle Model [5]

While MS models contain many parameters, several of them stand out due to their potential effects on model outcomes as determined by various sensitivity studies. The tendon slack length (TSL, or L_S^T) is the length beyond which a tendon must be stretched to generate force. A shorter L_S^T produces a higher force for a given tendon length as shown in the tendon force-strain curve in Figure 2. The moment arm length (MAL) is the distance between a muscle insertion point and the joint center. Longer MALs allow a muscle to generate a higher moment about the joint for a given force. Muscle fiber lengths can be normalized (NFL) with respect to their optimal muscle fiber length (L_O^M), the length at which a muscle is able to produce its peak force, indicating optimal active force production at a value of 1 as shown in the muscle curve in Figure 2. Finally, maximum isometric force (MIF) is related to muscle volume and indicates the force a muscle is capable of producing. MS models were generally found to have higher sensitivity to L_S^T and moderate to low sensitivity to MIF and L_O^M [6] [7] [8]. Meanwhile, perturbations in MALs were found to affect force generation in unperturbed muscles more than themselves [7] [9] [10].

Generic models are often based on the combination of data from multiple cadaveric studies, which introduces inconsistencies in the models themselves [11] and may thereby inaccurately represent live subjects, particularly those of varying size or fitness level. Models can be scaled to match the size of the subject being studied, however this method assumes properties scale linearly. For example, OpenSim's Scaling Tool adjusts length-dependent properties of muscles by the ratio of old to new body segment lengths. Medical imaging provides a possible, non-invasive solution to obtain personalized MS parameters of live subjects, thereby improving the accuracy of mathematical models and simulations [12]. To mitigate the drawbacks associated with MRI- or CT-based model creation, namely high costs and time consumption, efforts have been made to streamline the process making the use of medical imaging more practical in gait analysis. Advancements include: automated bone segmentation [13], atlas-based non-rigid image registration [14], and bone morphing [15].

Cerebral Palsy

One application of particular interest for personalized MS models is in gait analysis of children with cerebral palsy (CP). CP is a non-progressive but permanent disorder whose onset is attributed to disturbances during fetal or infant brain development [16]. Its primary symptoms are muscle imbalances such as abnormal muscle tone (usually hypertonia), muscle weakness, loss of muscle control, and impaired balance. Together, these contribute to a positive feedback loop-like behavior, where the consequent abnormal postures worsen muscle imbalances and cause unusual stresses on bones, leading to secondary symptoms such as bone deformities and joint instability or stiffness, further worsening postures [3].

Common deformities found in CP include pelvic and foot malrotations, femoral anteversion, tibial torsion, and lever arm disease, which is the decreased efficiency of force and torque transfer [3]. Common resulting gait patterns observed in ambulatory CP include jump knee gait, crouch gait, and stiff knee gait [3]. Several intervention strategies are available when managing ambulatory CP, such as pharmacology (eg. botulinum toxin-A injections), neurosurgery (eg. selective dorsal rhizotomy), muscle-tendon lengthening or transfer surgery, corrective osteotomy, and joint stabilization procedures [16].

Creating personalized MS models that better represent the subjects being evaluated can improve the accuracy of gait analysis outcomes. With increased reliability, these models can potentially be used for clinical decision making, predictive studies when planning intervention strategies, and establishing cause-effect relationships. The bone deformities and abnormal muscle characteristics of children with CP indicate that personalized MRI-based models may produce more accurate simulation outcomes and be an improvement over generic mathematical models.

Research Objective

The main purpose of this thesis is to evaluate the effect of MS model personalization on children with CP using MRI-based models in OpenSim. 3 types of models were used to simulate recorded gait of children with CP using OpenSim: scaled generic, MRI-based, and deformed generic models. Simulation outcomes were then analyzed to determine the differences between generic and personalized models. It was hypothesized that larger bone deformations will result in greater differences between the scaled generic model and the 2 personalized models. Additionally, simulation outcomes from the deformed model will lie between scaled generic and MRI-based model outcomes. Finally, it was also hypothesized that these differences will be reflective in variation between the parameters that MS models are most sensitive to.

The thesis begins by describing how gait data was collected, then outlines the steps taken in creating MS models, and processing and analyzing the data. Results are presented quantitatively and qualitatively for each parameter of interest. Connections between various parameters are made to establish cause-effect relationships and compared to available literature. Finally, conclusions are drawn and recommendations are provided.

2.0 Methods

2.1 Data Collection

The study initially involved 9 children with cerebral palsy identified as CP01 through CP09 who underwent magnetic resonance imaging (MRI) and had their gait analyzed by medical staff at Vrije Universiteit Medisch Centrum (VUmc) in Amsterdam, the Netherlands. Anthropometric data for these subjects are presented in Table 1, including femoral anteversion (FA) and tibial torsion (TT) angles measured manually using the Trochanteric Priminence Test [17] and Thigh-Foot Angle [18], respectively. Poor MRI resolution for CP01 and faulty force plate data for CP06 rendered full analysis infeasible and therefore these subjects were omitted from the study. In addition, bone deformation angles were not recorded for CP07, thus, only GS and MRI models were evaluated.

Table 1: Subject Data

Subject	Mass (kg)	Sex	Age	Height (m)	FA Angle (L | R)	TT Angle* (L | R)
VUMC-CP01	39.60	F	14	1.485	20° | 15°	-10° | -20°
VUMC-CP02	26.80	M	9	1.368	30° | 20°	5° | 15°
VUMC-CP03	32.00	M	8	1.320	20° | 15°	20° | 20°
VUMC-CP04	57.50	F	13	1.655	15° | 20°	5° | 0°
VUMC-CP05	49.50	M	13	1.640	20° | 10°	5° | 5°
VUMC-CP06	45.50	M	11	1.480	10° | 10°	-10° | 10°
VUMC-CP07	40.70	M	10	1.470	N/A	N/A
VUMC-CP08	48.20	M	12	1.596	15° | 15°	10° | 20°
VUMC-CP09	36.20	M	14	1.540	15° | 10°	10° | 15°

* Negative angle represents internal rotation

Gait measurements were done using a Gait Real-time Analysis Interactive Lab (GRAIL) system (by Motekforce Link), consisting of a dual-belt instrumented treadmill placed in a virtual environment projected on a 180° semi-cylindrical screen. Each patient was outfitted with markers placed on boney landmarks whose 3-dimensional positions were recorded over time using a Vicon motion capture system. The full marker set used can be found in the Appendix. Ground reaction forces (GRFs) were measured via force plates located under each belt of the GRAIL system. Muscle activity was also recorded using EMG for the muscles listed in Table 2 for both left and right legs (16 muscles total). These muscles were chosen because of their roles in gait and the fact that they are superficially located allowing for measurement. Due to file processing errors, EMG signals were lost for the left SOL, GAS, TA, and BFLH for CP02 and CP03.

Table 2: Muscles of Interest

Muscles of Interest			
GM	Gluteus Medius	**BFLH**	Biceps Femoris Long Head
RF	Rectus Femoris	**TA**	Tibialis Anterior
VL	Vastus Lateralis	**GAS**	Gastrocnemius Medius
ST	Semitendinosus	**SOL**	Soleus

2.2 Data Processing & Analysis

Collected data was processed using OpenSim with several steps prior to analysis to ensure data suitability and after to improve presentation of results. The entire procedure can be divided into 4 main parts:

1. Pre-processing collected data
2. Model Creation
3. OpenSim simulation and processing
4. Post-processing of OpenSim output

Figure 3 lays out the joints, muscles, and parameters of interest involved in this study. It should be noted that the GM muscle is divided into 3 parts in OpenSim to better represent its lines of action: GM1 is the anterior portion, GM3 is the posterior portion, and GM2 is located in between. 7 key outcomes and parameters pertaining to these structures were assessed after model simulation. Joint kinematics (angles) and kinetics (moments) served as general simulation outcomes while muscle activations helped describe which forces played contributing roles to these outcomes. Muscle moment arm lengths (MAL), normalized fiber lengths (NFL), tendon slack length (TSL), and maximum isometric forces (MIF) provided insight into the underlying mechanisms of muscle activations.

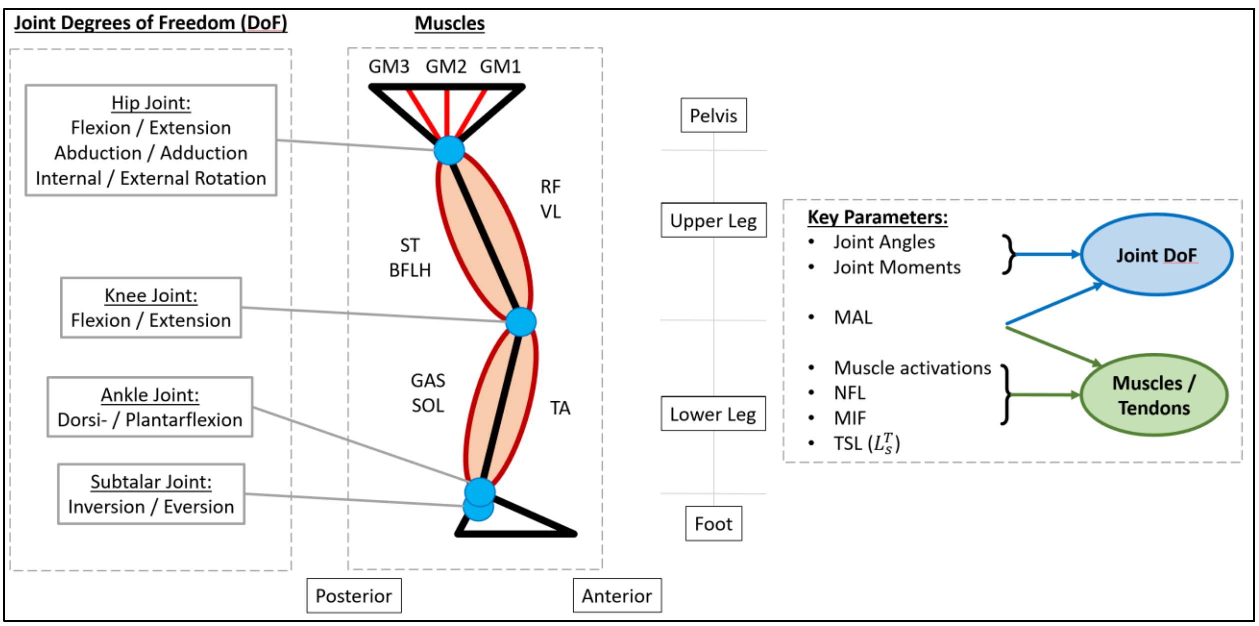

Figure 3: Simplified representation of the lower body with areas of interest

2.2.1 Pre-Processing

Pre-processing involved organizing and converting collected data so that it is useable in OpenSim. Due to measurement artefacts associated with the GRAIL system, force plate data from VUmc was filtered to eliminate force values in all directions if the vertical force was equal to or less than 30 N. EMG signals were filtered in the following manner:

i. Passing signal through a 2nd order high-pass filter with a cutoff frequency of 20 Hz
ii. Rectifying the signal
iii. Passing signal through a 2nd order low-pass filter with a cutoff frequency of 3 Hz

2.2.2 Model Creation

3 models of interest were analyzed for each patient:

a) Generic Scaled (GS) Model
Gait 2392 MS model scaled according to static pose data of each patient using OpenSim's algorithm

b) Tibial Torsion & Anteversion of Femur (TTAF) Model
GS model modified with 2 of the most prominent bone deformations found in CP

c) MRI Model
Created from magnetic resonance images of each patient

GS models were created using OpenSim's Scaling Tool which adjusts the body segment lengths of a generic model, Gait 2392, to fit the patient's static pose. The tool begins with the generic MS model and a virtual marker set based on 33 anatomical bony landmarks. Distances between specified virtual marker pairs are then scaled along with geometrical properties to match the corresponding distances in the experimental body markers. Non-uniform scaling was used to obtain different scaling factors for anterior-posterior, medial-lateral, and superior-inferior directions for certain segments. Marker pairs were selected based on anatomical positioning and through an iterative process aiming to minimize scaling errors; these pairs can be found in Appendix along with marker locations. Along with the body segment sizes, length-dependent properties such as tendon slack lengths and optimal muscles fiber lengths are scaled by the old-to-new segment length ratios. Body mass is also incorporated into the tool keeping proportions of body segment mass to total body mass constant. Finally, the MIF of all muscles was scaled separately using Equation 1, where m_i represents body mass and *gen* represents values from the Gait2392 model.

$$MIF_{new} = MIF_{gen} * \left(\frac{m_{new}}{m_{gen}}\right)^{2/3} \quad (1)$$

TTAF models were created similarly to GS models, with experimentally measured tibial torsion and femoral anteversion angles applied to the base Gait 2392 model. These bone deformations were implemented using a Matlab script developed by Hulda Jónasdóttir (previous Master student at TU Delft) based on algorithms by Arnold et al. [19], [20] for the femur and by Hicks et al. [21].

MRI models for all patients were previously prepared by Thomas Geijtenbeek and contain the same number of segments and muscles, and same joint models. MRI models were created by adapting the Gait2392 model using patient-specific muscle geometries (lines of action) and parameters from MRI data. MIFs are scaled using muscle volumes, segment lengths are scaled according to joint center locations, and muscle paths are adapted while L_S^T and L_O^M are scaled such that the ratio between them is constant. 24 virtual markers for these models, also described in the Appendix, were obtained from bony landmark positions located on the medical images. OpenSim's Scaling Tool was used to adjust the virtual marker positions with respect to the static pose data and adjust model mass; no geometrical changes were made to the model.

Scaling errors for all models can be found in the Appendix.

2.2.3 OpenSim Simulations & Processing

Gait data was initially assessed through visual inspection in OpenSim to determine the start and end times of 'good' strides. A good stride is defined as having a single foot making complete (not partial) contact per force plate without a stumble throughout the stride. The start time was taken as the first initial contact with a force plate (i.e. vertical force > 0) and the end time was taken as the time-step just prior to subsequent initial contact. With models created and gait data ready, 4 OpenSim tools were used to evaluate the good strides, summarized in Figure 4 below:

i. Inverse kinematics (IK)
The dynamic kinematics (dynamic.trc) were used to match virtual markers to experimental marker locations allowing the model to simulate the patient's gait motion. A file containing model kinematics (joint angles throughout gait simulation) was output.

ii. Inverse dynamics (ID)
GRFs (from dynamic.mot) were applied to the model at the calcaneus bones during its gait simulation obtained from IK. Both the kinematics and GRFs were low-pass filtered at 6 Hz. A file containing model kinetics (joint moments throughout gait simulation) was output.

iii. Static Optimization (SO)
Kinematics (from step i) and GRFs were used to determine muscle activation patterns under the criterion of minimizing sum of activations squared. Both input files use low-pass filters at 6 Hz (as in step ii).

iv. Analyze Tool
GRFs, history of muscle activations (output by step iii as 'controls'), as well as model states (output by step iii) were input into the tool and desired parameters are output.

The process was repeated for each model type (thus, 3 times per patient; twice for CP07).

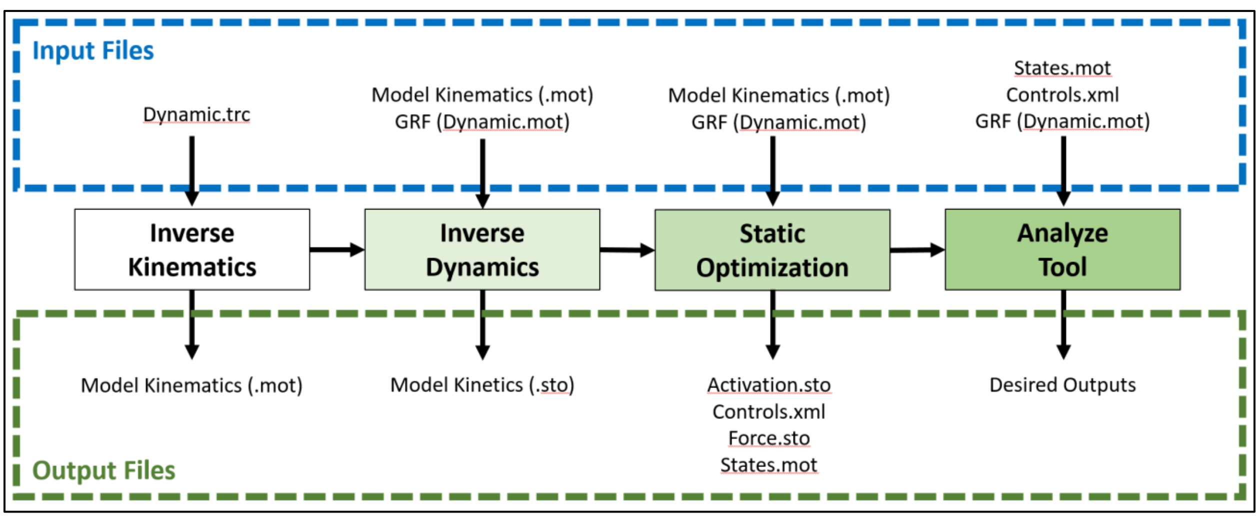

Figure 4: Process with OpenSim Tools

2.2.4 Post-Processing

OpenSim parameter results are typically presented over an analyzed time frame as shown in Figure 5.A. In post processing, time was normalized to stride duration using Equation 2, where t_i is time step i, t_0 is time of initial contact (represented by dotted lines Figure 5.A), and t_n is the time step prior to the next initial contact. Spline interpolation was then used to obtain parameter values corresponding to the normalized time for all good strides, as represented by the dotted lines in Figure 5.B, which were subsequently averaged to obtain 1 "patient-average" stride (solid line). The process was repeated for all 3 model types and compared as shown in Figure 5.C. Finally, the mean of these patient-average strides was taken across all patients to obtain 1 "overall-average" plot for each model type shown in Figure 5.D.

In the case of muscle activations, maximum and minimum constraints of 1 and 0, respectively, were implemented during the interpolation step. EMG signals were scaled with respect to the GS activation averaged over the entire stride as in Equation 3.

$$\tilde{t}_i = \frac{t_i - t_0}{t_n - t_0} * 100\% \tag{2}$$

$$Scaled\ EMG = EMG * \frac{(Average\ GS\ activation)_{0-100\%}}{(Average\ EMG)_{0-100\%}} \tag{3}$$

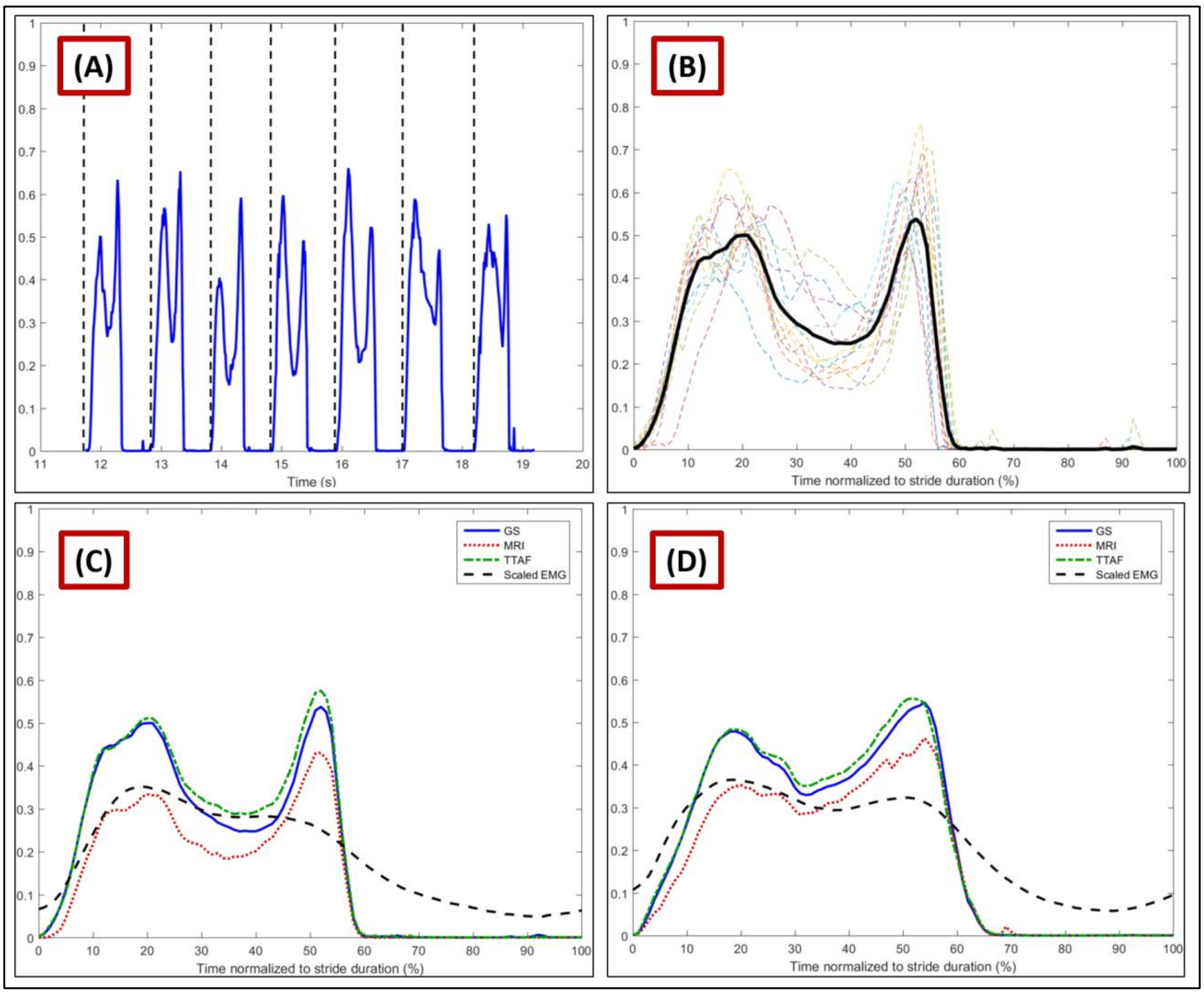

Figure 5: Example of post-processing done for right soleus muscle activations from VUmc data. (A) Typical OpenSim output over time for good strides, with initial contacts represented by dotted black lines. (B) All good strides for a specific model type (GS, MRI, or TTAF) normalized from 0 to 100% of a stride shown as dotted lines. The average of these good strides (dotted lines) is represented by the solid black line. (C) "Patient-average" strides for each model type for a single patient, along with average EMG scaled to the GS activation average. (D) "Overall-average" strides for each model type obtained from averaging the strides in (C) over all patients.

3.0 Results

A total of 20 models across 7 patients were completed, simulated, and assessed: 7 GS models, 7 MRI models, and 6 TTAF models. The analysis focused on comparing results from MRI and TTAF models based on subjects' personalized data, versus the outcomes of the linearly scaled GS model, which served as the baseline scenario. The comparisons are made using:

1. The absolute difference between GS and MRI model outcomes, denoted as dGM
2. The absolute difference between GS and TTAF model outcomes, denoted as dGT

Results are presented qualitatively and quantitatively through plots and tables, respectively, both of which utilize the normalized gait stride where 0% corresponds to initial contact and 100% to the end of terminal swing. Tables are color-coated using a common scale between GS vs MRI and GS vs TTAF comparisons, where darker entries represent larger differences. Outcomes for each parameter are first described using the overall average strides, then detailed through evaluation of patient average strides. This section divides comparisons into subsections (one for dGM and one for dGT) for each parameter, where differences are generally stated with respect to the outcomes from the generic model. For example, "higher moment arm length" in a dGM sub-section indicates the MRI model has a higher MAL than the GS model.

3.2 Joint Kinematics

Joint angles between the 3 models generally exhibited similar behavior over the gait cycle, but spanned different ranges. For example, knee joints underwent about 50° of flexion during the swing phase, but the GS model began at 15° while the MRI model began at 25°. Thus, general plot shapes appear consistent between models, but offset, unless otherwise noted. It is important to note that terms used when describing joint kinematics are relative and stated with respect to the GS model; for example, a "more extended knee" can mean the MRI (or TTAF) model's knee is still in flexion, but to a lesser degree. **Figure** 6 presents the joint angles for all 3 models.

Gait data collected from typically developing children by Schwartz et al. [1] has also been included with a 95% confidence interval as a reference. All 3 models generally exhibit high hip and knee flexion as well as ankle dorsiflexion, particularly in stance. The models also show higher hip abduction in mid to terminal swing and early stance, but high adduction in terminal stance. Hips show high internal rotations in terminal stance, with the exception of the MRI model's right leg which shows slight external rotation throughout. No healthy data was available for the subtalar angle, however TTAF models resulted in higher subtalar inversion in both legs when compared to the GS and MRI models.

Kinematic errors for each patient average over all good strides are included in the Appendix. Personalized models generally saw slight increases, with MRI and TTAF RMS errors larger by 2.4 mm and 0.9 mm, respectively. All average RMS errors were found to be below 1.7 cm.

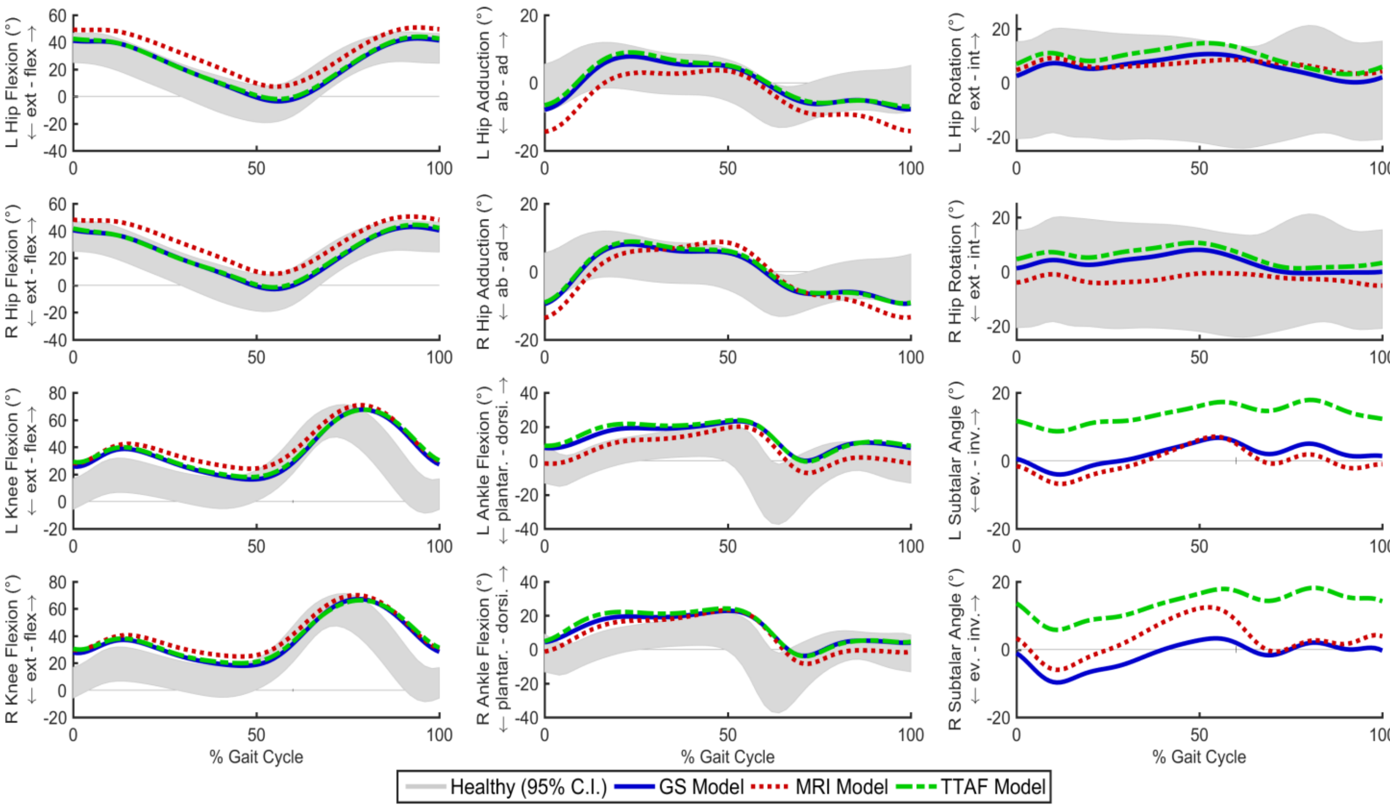

Figure 6: Joint kinematic comparisons using overall averages for each model type.

3.2.1 Kinematic Comparison with MRI Model

To investigate the kinematic differences between GS and MRI models, Table 1 provides a summary of the mean dGM for each joint which correspond to the plots in Figure 6 above. Largest differences were found in hip flexion and the left ankle angle where the MRI models experienced up to 11.2° more hip flexion from mid-stance until initial swing, and up to 9.1° less ankle dorsiflexion from mid-swing until loading response. The left ankle also exhibited a 5° larger range of motion (RoM) from pre-swing into initial swing. External rotation of the right hip, inversion of the right subtalar joint, and knee flexion in both legs were also noticeable differences and occurred during stance. The RoM was 7° smaller for the right hip rotation from pre-swing into initial swing and 5° larger for the right subtalar joint throughout stance, both of which are evident in the plot shapes in Figure 6.

Moderate increases were found in right ankle plantarflexion and left hip abduction in mainly loading response and terminal swing phases, with RoMs 5° larger during toe-off for the ankle and 6° larger during swing for the hip. The differences in the left hip rotation and subtalar angle are not well represented by the overall-average due to opposite joint motions between patients. For example, the left hip rotation RoM for CP02 is 7 – 18° with dGMs of 0 – 10°, while CP08 has a RoM from -6 – -16° with dGMs of 0 – 5°. Joint motion is fairly consistent between patients, with the largest differences occurring in stance for CP02 and 07. The left subtalar joint motion is consistent between GS and MRI models. Finally, right hip adduction exhibited the smallest, consistent differences.

Table 3: Mean dGM of overall-average joint angles for each phase of gait. Standard deviations range from 0 to 2.1°. All values are expressed in degrees (°).

Stride Phase		0 – 10%	10 – 30%	30 – 50%	50 – 60%	60 – 75%	75 – 87%	87 – 100%
R	hip flexion	8.7	11.0	11.2	11.2	10.5	8.9	7.7
	hip adduction	4.1	2.7	1.7	2.6	0.9	1.8	3.8
	Hip rotation	5.2	6.6	8.7	7.5	3.4	2.3	4.0
	knee angle	2.4	4.5	6.5	7.1	5.0	2.4	1.7
	ankle angle	5.0	3.0	0.8	0.4	3.3	5.5	5.7
	subtalar angle	4.2	4.7	8.0	8.5	2.7	0.7	2.6
L	hip flexion	8.4	9.9	11.1	10.8	10.5	8.9	8.1
	hip adduction	6.6	5.3	2.4	1.4	2.5	3.9	5.7
	Hip rotation	2.0	1.0	1.9	2.1	1.0	2.9	3.0
	knee angle	2.5	4.8	7.4	8.1	6.0	2.9	2.0
	ankle angle	9.1	7.7	4.9	3.3	5.9	8.2	9.1
	subtalar angle	2.3	2.6	1.0	0.3	2.2	3.3	3.2

3.2.2 Kinematic Comparison with TTAF Model

Table 4 provides mean dGT of overall-average joint angles during the gait cycle. The TTAF model exhibited smaller changes than the MRI, with the exception of the subtalar angle. During stance, hips were more adducted, knees less flexed, and ankles more dorsiflexed. Hips were more internally rotated and the subtalar joints more inverted throughout the gait cycle. CP03 was found to be the cause of the largest differences in both hip rotations and subtalar joints. In the left subtalar joint specifically, CP03 produced inversion while the other 2 models produced eversion through the majority of the gait cycle.

Table 4: Mean dGT of overall-average joint angles for each phase of gait. Standard deviations range from 0 to 1.0°. All values are expressed in degrees (°).

Stride Phase		0 - 10%	10 - 30%	30 - 50%	50 - 60%	60 - 75%	75 - 87%	87 - 100%
Ankle Angle	L	2.2	2.8	1.3	0.5	0.3	0.6	0.8
	R	2.2	2.9	1.8	0.8	0.1	0.3	0.3
Hip Add.	L	1.4	1.2	0.7	0.4	0.5	0.1	0.4
	R	0.5	0.7	0.7	0.6	0.5	0.2	0.1
Hip Flex.	L	0.9	0.1	0.5	1.6	1.3	0.7	1.2
	R	0.7	0.2	0.5	1.3	1.4	0.7	1.4
Hip Rot.	L	4.3	3.2	3.8	3.9	2.9	2.2	3.2
	R	3.3	2.8	2.9	2.3	2.0	1.9	2.5
Knee Angle	L	2.5	1.0	1.3	1.7	0.6	0.5	2.6
	R	2.0	0.9	1.5	1.9	0.8	0.7	2.7
Subtalar Angle	L	11.8	12.4	10.9	10.6	12.3	13.0	12.1
	R	15.1	15.2	13.8	14.5	15.9	16.1	15.0

3.3 Joint Moments

Much like the kinematic results, joint moments exhibited similar behaviours across all 3 models, with the main differences being in their magnitudes. Figure 7 shows the direct comparison between overall average joint moments referenced in the following subsections. Moments are expressed in [Nm / kg] to mediate differences caused by subject masses. Gait data collected from typically developing children by Schwartz et al. [1] has also been included with a 95% confidence interval as a reference. Hip and knee extension moments are high throughout mid-stance in all models and low through terminal-stance and pre-swing. Hip abduction moments are lower in terminal stance and pre-swing, and do not contain a second peak as the healthy data shows. Conversely, ankle plantarflexion moments show a peak in mid-stance which is not present in healthy children. No healthy data was available for hip rotation and subtalar joint moments, however MRI models had lower hip internal rotation moments in the left leg, while TTAF models exhibited noticeably lower subtalar inversion moments

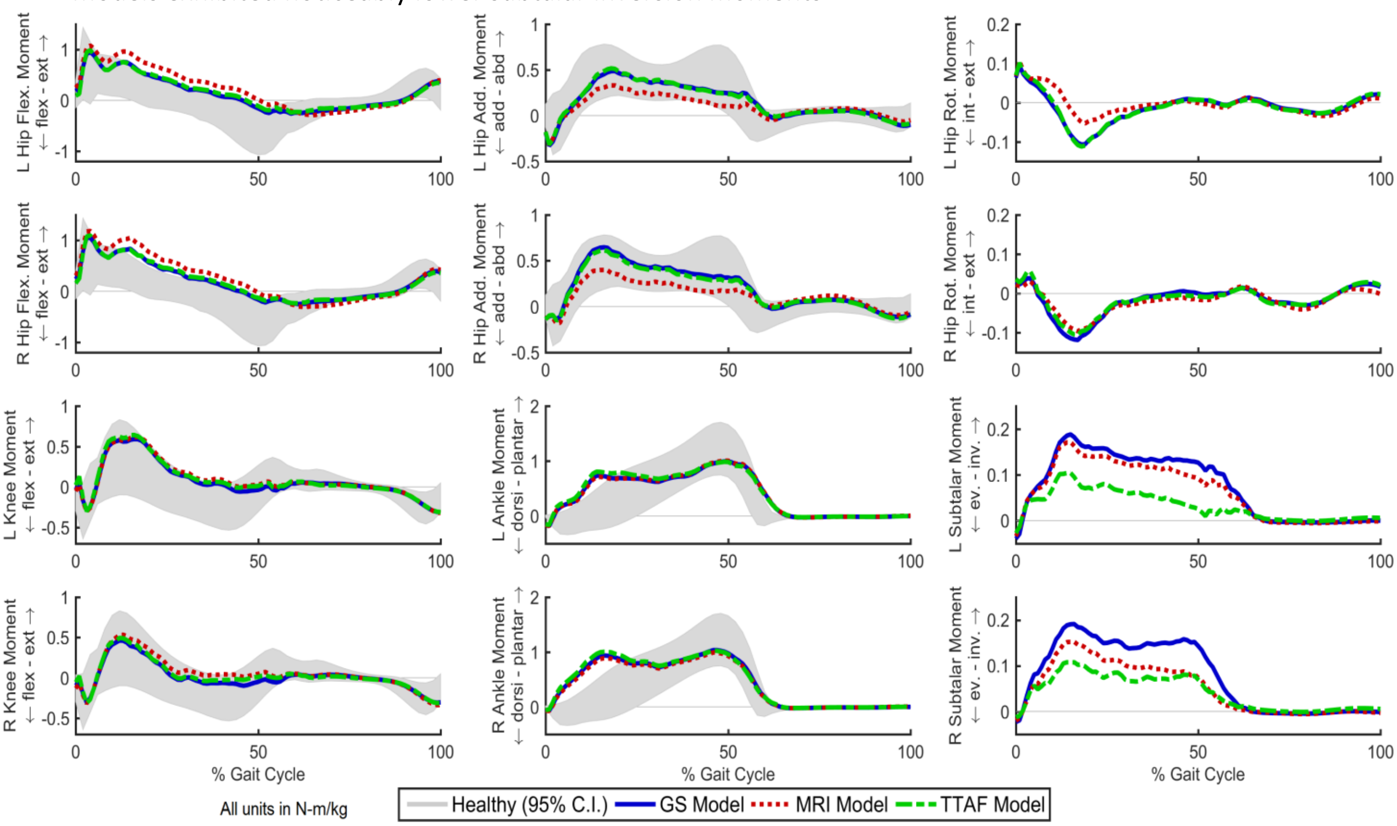

Figure 7: Joint Moments

3.3.1 Joint Moment Comparison with MRI Model

Table 5 provides mean dGM between GS and MRI overall-average joint moments during the gait cycle. Moments about the hip flexions experience the largest increase throughout the gait cycle in the MRI model. Meanwhile, hip adductions experience the largest decrease throughout stance, but see moderate increases during swing. Knee moments were larger in the MRI model, while subtalar moments were lower; most evident from mid-stance to toe-off in both joints. The right knee specifically saw a fairly large increase from 10 – 50%. Conversely, hip rotations and left ankle angle show the smallest differences in moments compared to the GS model. Right ankle moments were found to be lower throughout stance, but both ankle moments were similar to GS model results otherwise. Left hip rotation had a 5% delay in moment activity, compared to the GS model, during loading response, causing slightly higher moments from 0-15% then lower moments from 15-45%. Individual models have variations in ankle moments that are not represented by the average stride due to these moment acting in different directions between models. Right ankle moments were lower for all models except CP08 and CP09, and left ankle moments were lower for all models except CP03, 08 and 09.

Table 5: Mean dGM of overall-average joint moments for each phase of gait. Standard deviations range from 0.007 to 2.341. All values are expressed in [Nm/kg].

	Stride Phase	0 – 10%	10 – 30%	30 – 50%	50 – 60%	60 – 75%	75 – 87%	87 – 100%
R	Hip flexion	0.1307	0.1893	0.1510	0.0654	0.0750	0.0430	0.0261
	Hip adduction	0.0811	0.2071	0.1650	0.0881	0.0304	0.0351	0.0188
	Hip rotation	0.0130	0.0157	0.0125	0.0089	0.0048	0.0068	0.0099
	Knee angle	0.0234	0.0829	0.1019	0.0602	0.0040	0.0015	0.0127
	Ankle angle	0.0296	0.0391	0.0330	0.0345	0.0020	0.0010	0.0046
	Subtalar angle	0.0170	0.0377	0.0571	0.0460	0.0027	0.0006	0.0008
L	Hip flexion	0.1307	0.2037	0.1748	0.1171	0.0517	0.0442	0.0243
	Hip adduction	0.0342	0.1353	0.1348	0.1072	0.0186	0.0192	0.0317
	Hip rotation	0.0222	0.0455	0.0078	0.0072	0.0019	0.0051	0.0080
	Knee angle	0.0113	0.0295	0.0555	0.0432	0.0086	0.0031	0.0046
	Ankle angle	0.0110	0.0153	0.0160	0.0105	0.0039	0.0015	0.0035
	Subtalar angle	0.0062	0.0155	0.0213	0.0258	0.0035	0.0014	0.0014

3.3.2 Joint Moment Comparison with TTAF Model

Table 6 provides mean dGT of overall-average joint moments during the gait cycle. TTAF models generally exhibited larger variations in the knee, ankle, and subtalar joints, but lower in the hip compared to MRI results. Ankle and knee moments were higher than the GS model during first half of gait cycle. Hip adduction experienced slightly higher values in mid stance but lower in terminal stance on the left side, while right hip experienced lower moments. Hip flexion moment was slightly higher throughout stance but lower in swing. Left hip rotation moments were similar to the GS model, while the right hip saw small moments in mid stance but larger moments in other phases. The lower subtalar joint moments were mainly caused by CP03, 08, and 09.

Table 6: Mean dGT of overall-average joint moments for each phase of gait. Standard deviations range from 0.017 to 1.403. All values are expressed in [Nm/kg].

	Stride Phase	0 – 10%	10 – 30%	30 – 50%	50 – 60%	60 – 75%	75 – 87%	87 – 100%
R	Hip flexion	0.0332	0.0192	0.0287	0.0200	0.0183	0.0090	0.0237
	Hip adduction	0.0181	0.0277	0.0308	0.0188	0.0089	0.0051	0.0103
	Hip rotation	0.0113	0.0095	0.0048	0.0041	0.0029	0.0015	0.0027
	Knee angle	0.0283	0.0219	0.0429	0.0426	0.0141	0.0064	0.0057
	Ankle angle	0.0514	0.0579	0.0114	0.0375	0.0057	0.0023	0.0022
	Subtalar angle	0.0296	0.0760	0.0753	0.0447	0.0050	0.0041	0.0062
L	Hip flexion	0.0309	0.0191	0.0345	0.0420	0.0268	0.0080	0.0223
	Hip adduction	0.0180	0.0152	0.0077	0.0146	0.0096	0.0067	0.0117
	Hip rotation	0.0081	0.0029	0.0011	0.0007	0.0034	0.0014	0.0034
	Knee angle	0.0449	0.0259	0.0333	0.0324	0.0148	0.0079	0.0029
	Ankle angle	0.0470	0.0740	0.0242	0.0324	0.0079	0.0017	0.0018
	Subtalar angle	0.0254	0.0791	0.0851	0.0814	0.0106	0.0033	0.0058

3.4 Muscle Activations

Muscle activity variations between models mainly occurred during the stance phase, with highest changes occurring in the MRI model. Overall average muscle activations and scaled EMG signals are depicted in Figure 8 and Figure 9 for the right and left legs, respectively. To better describe findings, muscle names mentioned in this section may be equipped with a –R or –L suffix to signify right and left legs, respectively.

3.4.1 Muscle Activation Comparison with MRI Model

The quadriceps (VL, RF) were generally affected least throughout gait, with the exception of RF during pre-swing. On the other hand, the highest differences occurred in several different muscles at various times during the stance. Broken down by phase, these were:

Loading Response:	ST	BFLH	TA-R		
Mid-Stance:	SOL	GM-R	GM1-L	ST	BFLH
Terminal Stance:	SOL-L	GM-R	GM1-L		
Toe-Off:	SOL	GAS	RF-R		

BFLH and ST had higher activations throughout the gait cycle, meanwhile GM and SOL were lower during stance and push off, and VL was lower during loading response and mid stance. GAS-L activations were slightly higher during loading response and mid stance while GAS-R was lower during mid stance, and both were noticeably larger at pre-swing and toe-off. TA was moderately higher during both toe-off and initial swing phases for the right leg, but only the swing phase for the left leg. TA had higher activations at initial contact in both legs, but lower activations during stance in the left leg. RF activations were higher in pre-swing and initial swing phases, but lower in mid stance. Table 7 summarizes these differences using mean dGM of overall-average muscle activations during the gait cycle. Since muscle activation values varied more than other parameters, even within a single gait phase, a more comprehensive summary of standard deviations corresponding to this table are included in the Appendix. The standard deviations typically coincide with muscle activations; higher standard deviations are associated with higher activations (eg. 0.0895 for ST-L at mid stance) and lower standard deviations with lower activations (eg. 0.0023 for GAS-R at terminal swing).

Activations for most muscles studied generally showed consistent activation patterns to those depicted by the overall-averages. GAS, RF, and T-L were the exceptions and varied between patients. Additionally, high differences seen in TA activations from 0 – 10% were mainly caused by CP07 activations. Removing CP07 from the averages reduces dGM for TA- L to approximately 0.0669 and TA-R to 0.0192, and keeps remaining values relatively consistent.

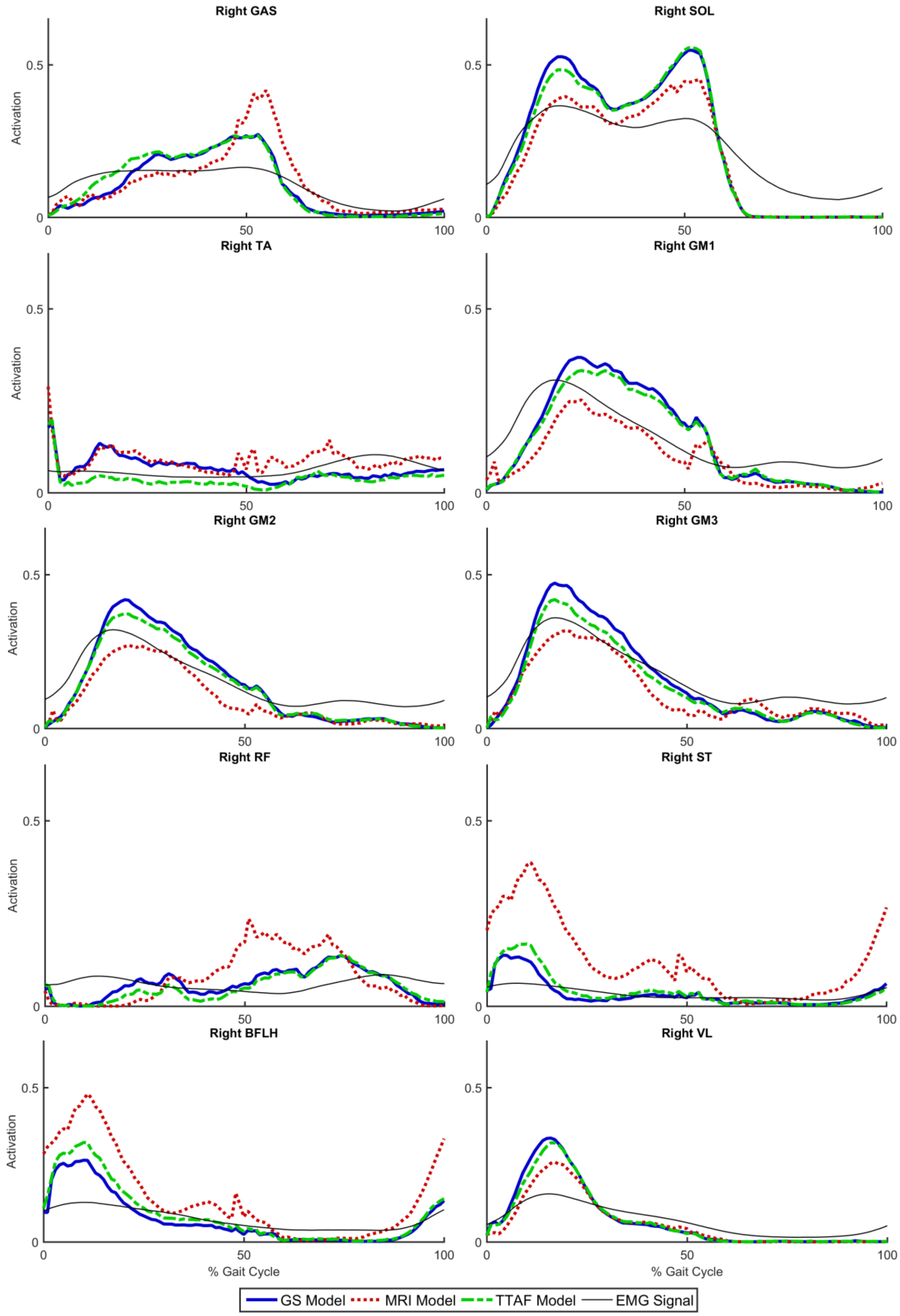

Figure 8: Overall average muscle activations and scaled EMG signals for the right leg

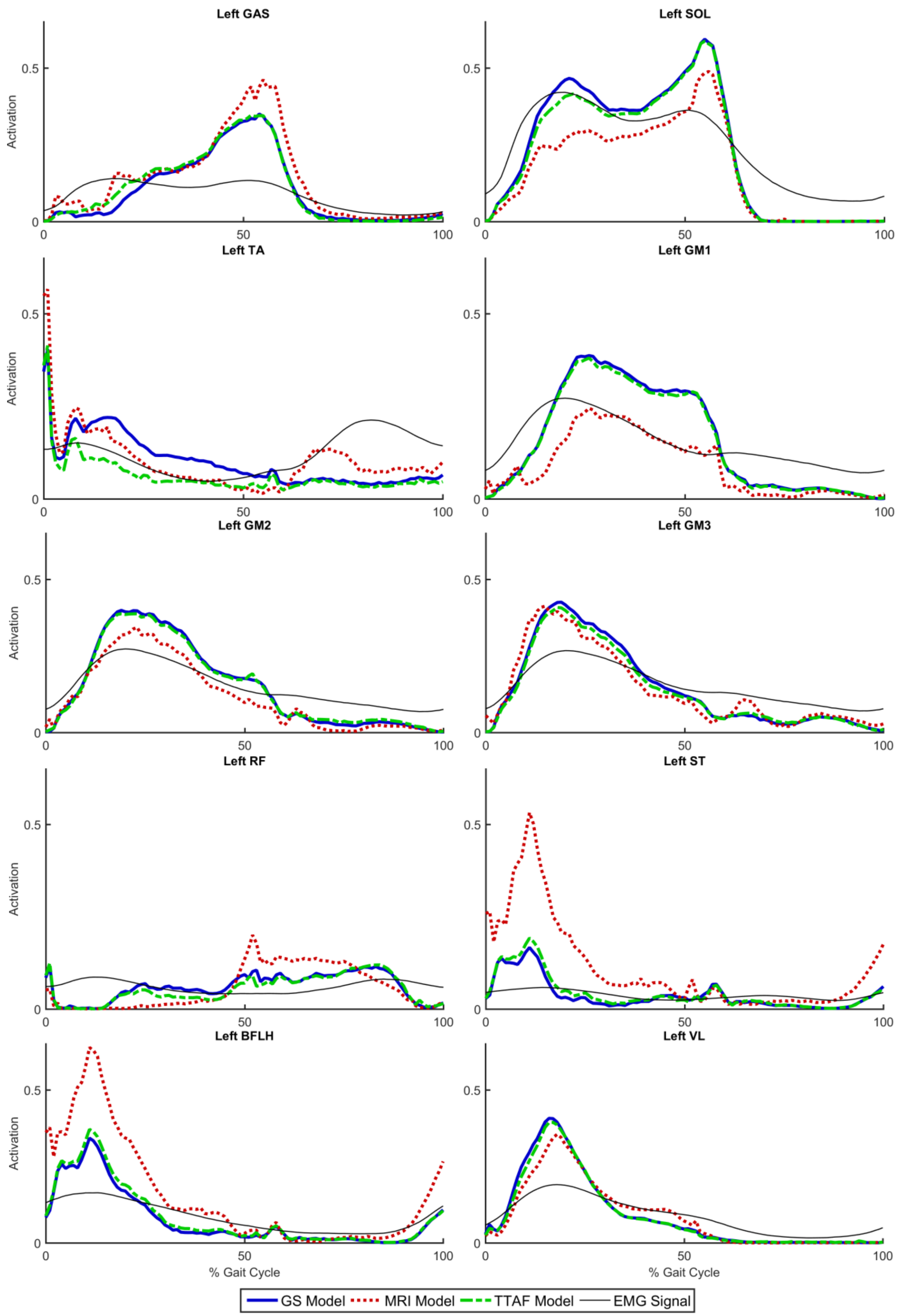

Figure 9: Overall average muscle activations and scaled EMG signals for the left leg

Table 7: Mean dGM of overall-average muscle activations for each phase of gait. Standard deviations can be found in the Appendix.

Stride Phase		0 - 10%	10 - 30%	30 - 50%	50 - 60%	60 - 75%	75 - 87%	87 - 100%
R	GAS	0.0132	0.0270	0.0528	**0.1416**	0.0564	0.0074	0.0060
	SOL	0.0398	0.1009	0.0502	0.0636	0.0037	0.0002	0.0003
	TA	0.0608	0.0103	0.0105	0.0554	0.0660	0.0316	0.0290
	GM1	0.0274	0.1029	**0.1215**	0.0461	0.0166	0.0078	0.0073
	GM2	0.0256	**0.1319**	0.1050	0.0538	0.0048	0.0070	0.0046
	GM3	0.0275	**0.1527**	0.1016	0.0515	0.0203	0.0060	0.0136
	RF	0.0076	0.0341	0.0422	**0.1114**	0.0519	0.0223	0.0103
	ST	**0.1998**	**0.1618**	0.0644	0.0457	0.0060	0.0204	0.0878
	BFLH	**0.1571**	0.1138	0.0520	0.0282	0.0035	0.0179	0.0859
	VL	0.0417	0.0400	0.0085	0.0089	0.0021	0.0022	0.0010
L	GAS	0.0281	0.0327	0.0162	**0.1240**	0.0471	0.0063	0.0040
	SOL	0.0288	**0.1337**	0.1048	**0.1247**	0.0142	0.0006	0.0003
	TA	**0.1410**	0.0335	0.0372	0.0177	0.0553	0.0414	0.0221
	GM1	0.0187	**0.1275**	**0.1237**	0.0974	0.0256	0.0120	0.0059
	GM2	0.0117	0.0752	0.0653	0.0571	0.0153	0.0162	0.0055
	GM3	0.0298	0.0528	0.0484	0.0280	0.0156	0.0046	0.0119
	RF	0.0107	0.0272	0.0298	0.0732	0.0381	0.0238	0.0090
	ST	**0.1972**	**0.1785**	0.0356	0.0154	0.0064	0.0129	0.0501
	BFLH	**0.1877**	**0.1630**	0.0507	0.0140	0.0047	0.0100	0.0615
	VL	0.0349	0.0479	0.0293	0.0110	0.0022	0.0024	0.0005

3.4.2 Muscle Activation Comparison with TTAF Model

TTAF muscle activations were generally found to be similar to those from the GS models, both in shape and magnitude. BFLH had slightly higher activations during stance, which were more evident on the right side. Activations were also higher for ST-R during stance, SOL-R in terminal stance, and GAS in mid stance. Conversely, lower activations were present in GM throughout stance, and GAS-R and RF in terminal stance. Table 8 summarizes these differences using mean dGT of overall-average muscle activations during the gait cycle. Since muscle activations were more varied than other parameters, even within a single gait phase, a more comprehensive summary of standard deviations corresponding to this table are included in the Appendix.

Table 8: Mean dGT of overall-average muscle activations for each phase of gait. Standard deviations can be found in the Appendix.

Stride Phase		0 - 10%	10 - 30%	30 - 50%	50 - 60%	60 - 75%	75 - 87%	87 - 100%
R	GAS	0.0138	0.0495	0.0166	0.0289	0.0074	0.0035	0.0063
	SOL	0.0049	0.0085	0.0250	0.0276	0.0033	0.0001	0.0003
	TA	0.0410	0.0527	0.0345	0.0127	0.0036	0.0079	0.0120
	GM1	0.0023	0.0322	0.0240	0.0080	0.0086	0.0017	0.0013
	GM2	0.0095	0.0496	0.0353	0.0126	0.0095	0.0019	0.0014
	GM3	0.0257	0.0803	0.0636	0.0215	0.0091	0.0019	0.0031
	RF	0.0045	0.0229	0.0220	0.0026	0.0162	0.0076	0.0104
	ST	0.0250	0.0226	0.0113	0.0095	0.0026	0.0010	0.0075
	BFLH	0.0373	0.0345	0.0222	0.0092	0.0028	0.0016	0.0037
	VL	0.0100	0.0158	0.0104	0.0013	0.0007	0.0012	0.0006
L	GAS	0.0072	0.0408	0.0182	0.0067	0.0081	0.0027	0.0063
	SOL	0.0031	0.0026	0.0103	0.0189	0.0073	0.0001	0.0005
	TA	0.0485	0.1093	0.0661	0.0227	0.0062	0.0060	0.0120
	GM1	0.0008	0.0080	0.0033	0.0047	0.0036	0.0007	0.0015
	GM2	0.0039	0.0043	0.0076	0.0071	0.0109	0.0074	0.0034
	GM3	0.0027	0.0177	0.0300	0.0145	0.0092	0.0071	0.0098
	RF	0.0052	0.0077	0.0207	0.0114	0.0141	0.0069	0.0045
	ST	0.0118	0.0142	0.0056	0.0048	0.0035	0.0012	0.0030
	BFLH	0.0181	0.0154	0.0104	0.0065	0.0021	0.0019	0.0024
	VL	0.0069	0.0072	0.0078	0.0011	0.0009	0.0012	0.0013

3.4.3 Comparisons to EMG Recordings

While EMG signals cannot be compared quantitatively, their onsets and offsets can be used to make qualitative judgements. Accordingly, EMG signal patterns for BFLH, GM, GAS, SOL, and VL agree with muscle activations predicted by the OpenSim model simulations. TA agreement varied between patients, for example: CP04 saw similar activity across all models and EMG; while CP09's swing phase had low activations in the GS and TTAF models, moderate activation in the MRI model, but a high EMG signal.

The agreement between EMG and model predictions is questionable for ST and RF muscles. ST-L EMG signals produce a small peak at about 70% which is only predicted by CP02 and CP05. Model RF activations exhibit a similar "peak-valley-peak" pattern present in the EMG signal, but offset. Peaks in the models occur from 20 – 40% and from 40 – 90%, but in EMG these occur at 0 – 30% and 70 – 100%.

3.5 Muscle Moment Arm Lengths

The largest MAL differences between the GS-MRI models were found with respect to hip flexion, followed by hip adductors, muscles involved in ankle dorsi- / plantarflexion, and the left ST and BFLH with respect to the knee. These results vary greatly compared to those from the GS-TTAF comparison where the largest differences occurred in the knee, followed by moderate variations in the GAS and SOL with respect to the subtalar angle. Figure 10 and Figure 11 show the moment arm lengths for left and right legs, respectively.

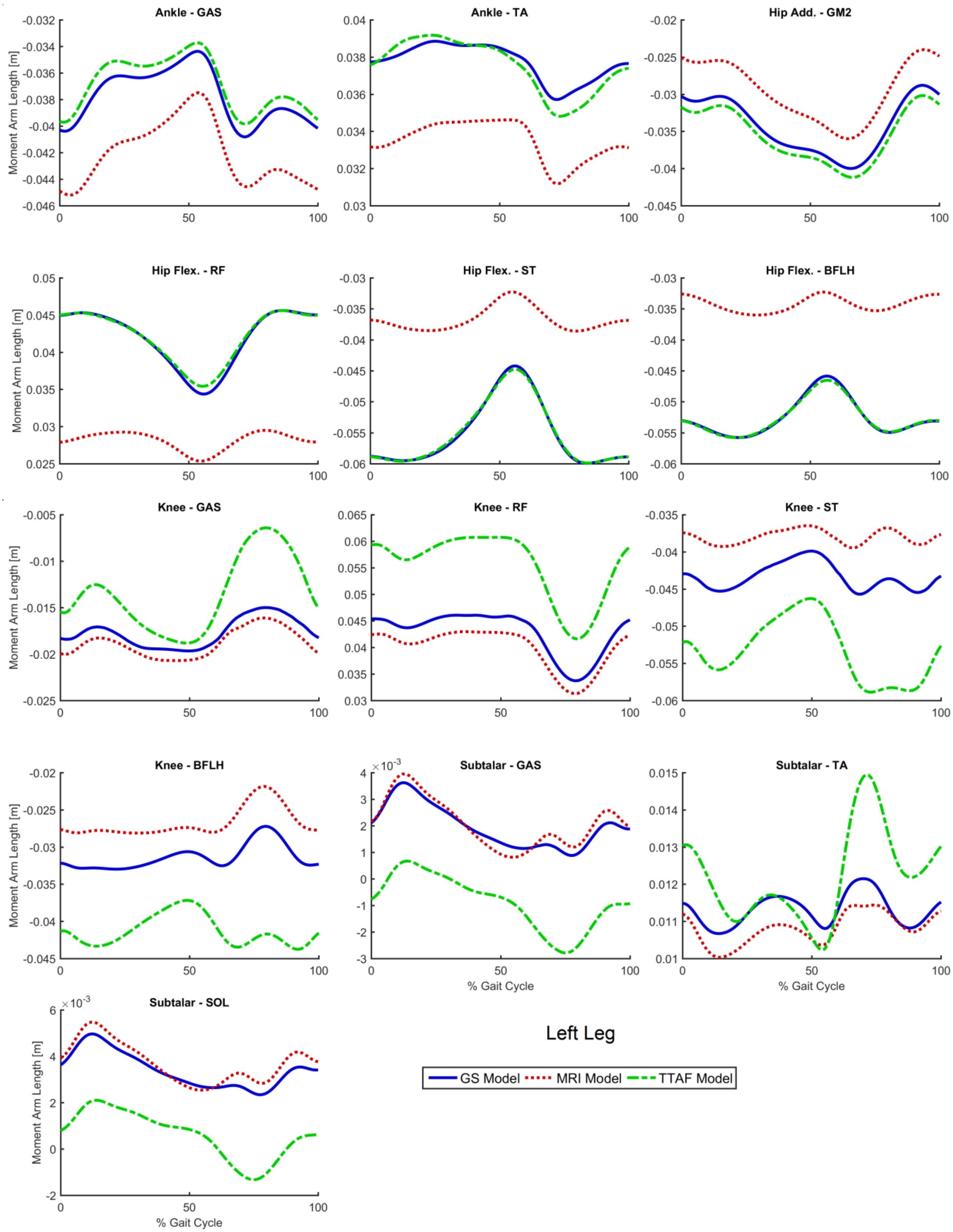

Figure 10: Moment Arm lengths for the left leg.

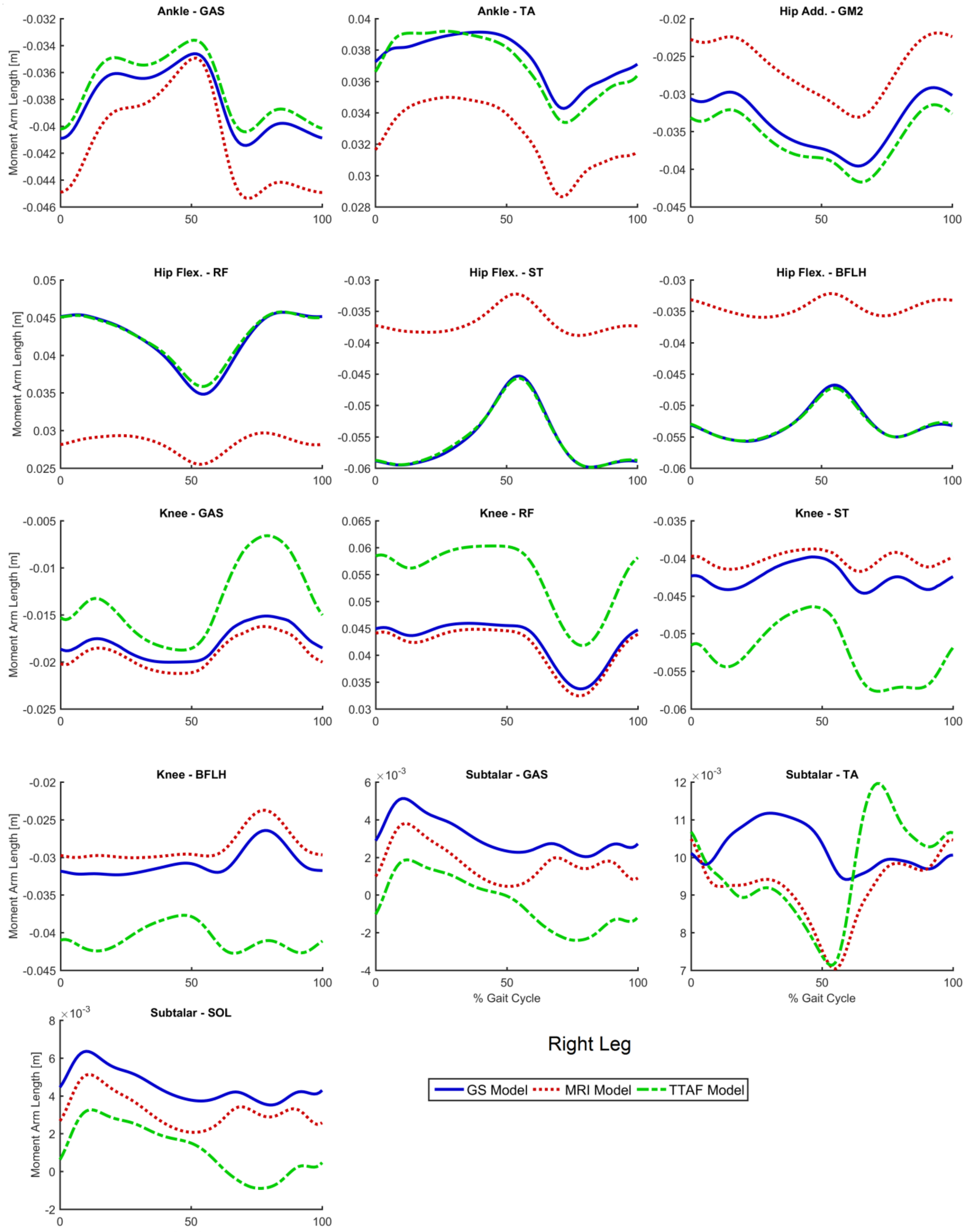

Figure 11: Moment arm lengths for the right leg

3.5.1 MAL Comparison with MRI Model

GAS muscles were found to have longer moment arm lengths with respect to the ankle and knee joints. GAS-R also exhibited a range of motion about 3 mm larger from toe-off to initial swing for the ankle. The GAS-L MAL for the subtalar joint was slightly longer (except from about 40 – 60%), but GAS-R was shorter throughout. TA lengths were shorter with respect to the ankle and left subtalar joints. For the right subtalar joint, the TA MAL was briefly longer from -10 – 5% (from the end of terminal swing until halfway through loading response) then shortened until stance and stayed relatively constant until terminal stance, meanwhile the GS length increased during this time. MALs from both models then shortened until toe-off, but the MRI muscle's range of motion was about 2 mm longer. GM2 moment arms with respect to hip adduction were shorter over the entire gait cycle. The same was true for BFLH, RF, and ST muscles with respect to the knee joint. Hip flexion muscles all had shorter MALs, as well as smaller ranges of motion by about 6 mm from terminal stance to toe-off. The SOL-R MAL with respect to the subtalar joint was lower over the entire cycle, while the SOL-L was lower only during 40 – 60% and higher elsewhere. Table 9 summarizes these differences.

Table 9: Mean dGM of overall-average MALs for each phase of gait. Standard deviations range from 0.011 to 2.431 [mm]. All values a given in [mm].

Stride Phase →		0 – 10%	10 – 30%	30 – 50%	50 – 60%	60 – 75%	75 – 87%	87 – 100%
DOF & Muscle ↓								
Ankle Angle L	**GAS**	5.064	5.212	3.918	3.161	3.576	4.352	4.756
	TA	4.613	4.490	4.083	3.637	4.150	4.243	4.311
Ankle Angle R	**GAS**	3.897	2.900	1.206	0.709	3.275	4.292	4.286
	TA	4.959	3.873	4.431	5.165	5.551	5.265	5.400
Hip Add. L	**GM2**	5.191	5.003	5.011	4.021	4.201	4.792	4.853
Hip Add. R	**GM2**	7.786	7.605	7.753	6.616	6.616	6.949	7.301
Hip Flex L	**RF**	16.918	15.183	11.611	9.196	11.292	15.526	16.975
	ST	21.914	20.484	16.145	12.274	15.485	20.932	21.939
	BFLH	20.519	20.098	16.972	13.856	16.013	19.844	20.391
Hip Flex R	**RF**	16.738	14.843	11.729	9.474	11.896	15.737	16.948
	ST	21.540	20.277	16.805	13.336	16.672	20.903	21.524
	BFLH	20.202	19.961	17.484	14.778	16.902	19.716	19.911
Knee L	**GAS**	1.458	1.005	1.053	0.896	0.969	1.190	1.498
	RF	2.836	3.244	3.079	3.189	3.180	2.367	2.544
	ST	5.656	5.586	4.054	3.631	6.003	6.781	6.198
	BFLH	4.650	4.930	3.754	3.572	5.356	5.302	4.921
Knee R	**GAS**	1.280	0.870	1.072	0.876	1.029	1.202	1.391
	RF	0.916	1.377	1.066	1.339	1.738	1.123	0.833
	ST	2.619	2.363	1.316	1.407	2.942	3.168	2.867
	BFLH	2.175	2.306	1.471	1.748	2.874	2.571	2.263
Subtalar L	**GAS**	0.127	0.253	0.201	0.344	0.277	0.348	0.353
	TA	0.424	0.682	0.737	0.451	0.584	0.159	0.162
	SOL	0.368	0.419	0.159	0.128	0.410	0.522	0.562
Subtalar R	**GAS**	1.683	1.390	1.843	1.698	0.907	0.641	1.268
	TA	0.381	1.484	2.198	2.491	0.745	0.112	0.215
	SOL	1.558	1.265	1.670	1.577	0.914	0.638	1.205

3.5.2 MAL Comparison with TTAF Model

GAS moment arms with respect to the ankle were shorter, while TA lengths increased slightly quicker during the first half of stance, resulting in longer MALs from about 5 to 30%, but shorter at other times. GM2 lengths with respect to hip adduction were found to be shorter. Hip flexion MALs were similar over the gait cycle, with TTAF lengths being slightly longer just prior to, during, and just after the toe-off phase. For the knee joint: BLFH and ST had longer MALs throughout gait and a larger range from stance until push off, but lower during swing; GAS had shorter lengths but exhibited a larger range throughout; and RF MALs were longer, with a larger range during swing. With respect to the subtalar joints, GAS moment arms from TTAF models were mainly in the opposite direction of the GS model moment arms, except during mid-stance. Thus, the moment arms appeared to be momentarily parallel to the direction of motion (MAL = 0) at the beginning and at the end of mid stance for the left leg, or terminal stance for the right leg. The SOL MALs were shorter overall and went in the opposite direction during initial and mid-swing, once again resulting in MAL = 0 during these transitions between directions. TA-L moment arms were briefly shorter from about 35% until toe-off, but longer at all other times. The muscle also had a larger range at loading response by 1 mm and from pre- to mid-swing by about 4.5 mm. TA-R moment arms were more similar to those from the MRI model, but with an even larger range during initial swing. Table 10 summarizes these differences.

Table 10: Mean dGT of overall-average MALs for each phase of gait. Standard deviations range from 0.004 to 2.052 [mm]. All values a given in [mm].

Stride Phase → / **DOF & Muscle ↓**		**0 – 10%**	**10 – 30%**	**30 – 50%**	**50 – 60%**	**60 – 75%**	**75 – 87%**	**87 – 100%**
Ankle Angle L	**MGAS**	0.854	1.134	0.769	0.665	0.902	0.857	0.825
	TA	0.245	0.446	0.097	0.337	0.724	1.001	0.452
Ankle Angle R	**MGAS**	0.867	1.150	1.014	0.982	1.017	1.065	0.842
	TA	0.463	0.534	0.311	0.843	0.895	1.059	0.746
Hip Add. L	**GM2**	1.480	1.230	1.083	0.982	1.242	1.538	1.400
Hip Add. R	**GM2**	2.534	2.261	1.681	1.332	2.260	2.680	2.361
Hip Flex L	**RF**	0.040	0.086	0.291	0.991	0.681	0.062	0.060
	ST	0.096	0.173	0.318	0.502	0.188	0.102	0.009
	BFLH	0.091	0.096	0.178	0.627	0.217	0.092	0.081
Hip Flex R	**RF**	0.087	0.098	0.414	1.012	0.699	0.101	0.097
	ST	0.076	0.246	0.252	0.329	0.193	0.034	0.097
	BFLH	0.068	0.074	0.170	0.466	0.261	0.016	0.201
Knee L	**MGAS**	3.544	3.800	1.446	1.593	5.916	8.359	5.634
	RF	**13.567**	**13.312**	**14.670**	**14.539**	**11.175**	8.230	**11.601**
	ST	**9.613**	**9.630**	7.000	7.079	**11.621**	**14.420**	**11.751**
	BFLH	**9.443**	**9.599**	7.017	7.187	**11.636**	**14.214**	**11.452**
Knee R	**MGAS**	3.648	3.524	1.641	2.467	6.502	8.309	5.688
	RF	**13.151**	**13.065**	**14.382**	**13.918**	**10.533**	8.273	**11.232**
	ST	**9.418**	**9.315**	6.949	7.753	**12.374**	**14.324**	**11.598**
	BFLH	**9.321**	**9.331**	7.124	7.923	**12.424**	**14.225**	**11.325**
Subtalar L	**MGAS**	2.989	2.710	2.258	2.199	3.420	3.476	3.066
	TA	1.584	0.417	0.220	0.442	1.988	1.869	1.383
	SOL	2.933	2.620	2.199	2.143	3.395	3.453	3.018
Subtalar R	**MGAS**	3.648	2.948	2.517	2.845	4.455	4.364	3.988
	TA	0.331	1.641	2.489	2.239	1.476	1.029	0.604
	SOL	3.517	2.775	2.400	2.725	4.392	4.323	3.926

3.6 Normalized Muscle Fiber Lengths

The NFLs for all muscles in the personalized models follow the same patterns as those in the GS model. Despite these similarities, which muscles were most affected and at what times varies noticeably between dGM and dGT results. Additional tables are included in the Appendix indicating the distance of each model's NFLs from a value of 1 (length of optimal force generation).

3.6.1 NFL Comparisons with MRI Model

GAS values were shorter for the MRI models over the gait cycle, and the muscle experienced the highest differences throughout the swing phase until the end of mid stance, especially in the left leg. The results for SOL are similar to that of GAS, with the exception of the right side which reached slightly larger NFL at terminal stance and push-off. TA and GM-R values were higher throughout. GM-L segments had smaller NFLs at the start and end of the stride, but larger values over the mid-section; GM1-L was higher during terminal stance, GM2-L from 20 – 75%, and GM3-L from 15 – 80%. GM1 also had slower length changes in terminal stance then quicker at push-off. RF was lower from 40 – 75%, while ST (30 – 80%), BFLH (30 – 80%), and VL (20 – 65%) had higher NFLs. Table 11 summarizes these findings and Figure 12 shows that from the largest differences: GAS, SOL, BFLH during swing, and GM1-L had NFLs farther from 1; meanwhile, GM1-R, BFLH during loading response, and TA-L had values closer to 1.

Table 11: Mean dGM of overall-average NFLs for each phase of gait. Standard deviations range from 0.001 to 0.025.

Stride Phase		0 – 10%	10 – 30%	30 – 50%	50 – 60%	60 – 75%	75 – 87%	87 – 100%
R	GAS	0.093	0.070	0.044	0.040	0.081	0.094	0.100
	SOL	0.067	0.031	0.008	0.008	0.043	0.069	0.075
	TA	0.030	0.023	0.006	0.003	0.015	0.031	0.031
	GM1	0.068	0.071	**0.128**	**0.120**	0.074	0.046	0.061
	GM2	0.035	0.048	0.068	0.061	0.056	0.042	0.036
	GM3	0.012	0.029	0.039	0.033	0.054	0.041	0.018
	RF	0.062	0.029	0.007	0.017	0.015	0.028	0.069
	ST	0.048	0.017	0.007	0.024	0.019	0.017	0.052
	BFLH	0.093	0.041	0.013	0.045	0.030	0.041	0.100
	VL	0.003	0.015	0.042	0.041	0.014	0.025	0.016
L	GAS	**0.156**	**0.135**	0.095	0.075	**0.128**	**0.147**	**0.153**
	SOL	**0.114**	0.074	0.034	0.011	0.065	0.094	**0.106**
	TA	0.068	0.061	0.040	0.028	0.045	0.062	0.071
	GM1	0.079	0.063	0.012	0.009	0.035	0.069	0.074
	GM2	0.029	0.013	0.026	0.025	0.011	0.010	0.021
	GM3	0.025	0.016	0.036	0.034	0.032	0.012	0.012
	RF	0.059	0.028	0.006	0.023	0.033	0.015	0.052
	ST	0.044	0.016	0.014	0.030	0.035	0.013	0.038
	BFLH	0.086	0.037	0.024	0.057	0.058	0.022	0.076
	VL	0.015	0.013	0.038	0.042	0.021	0.041	0.031

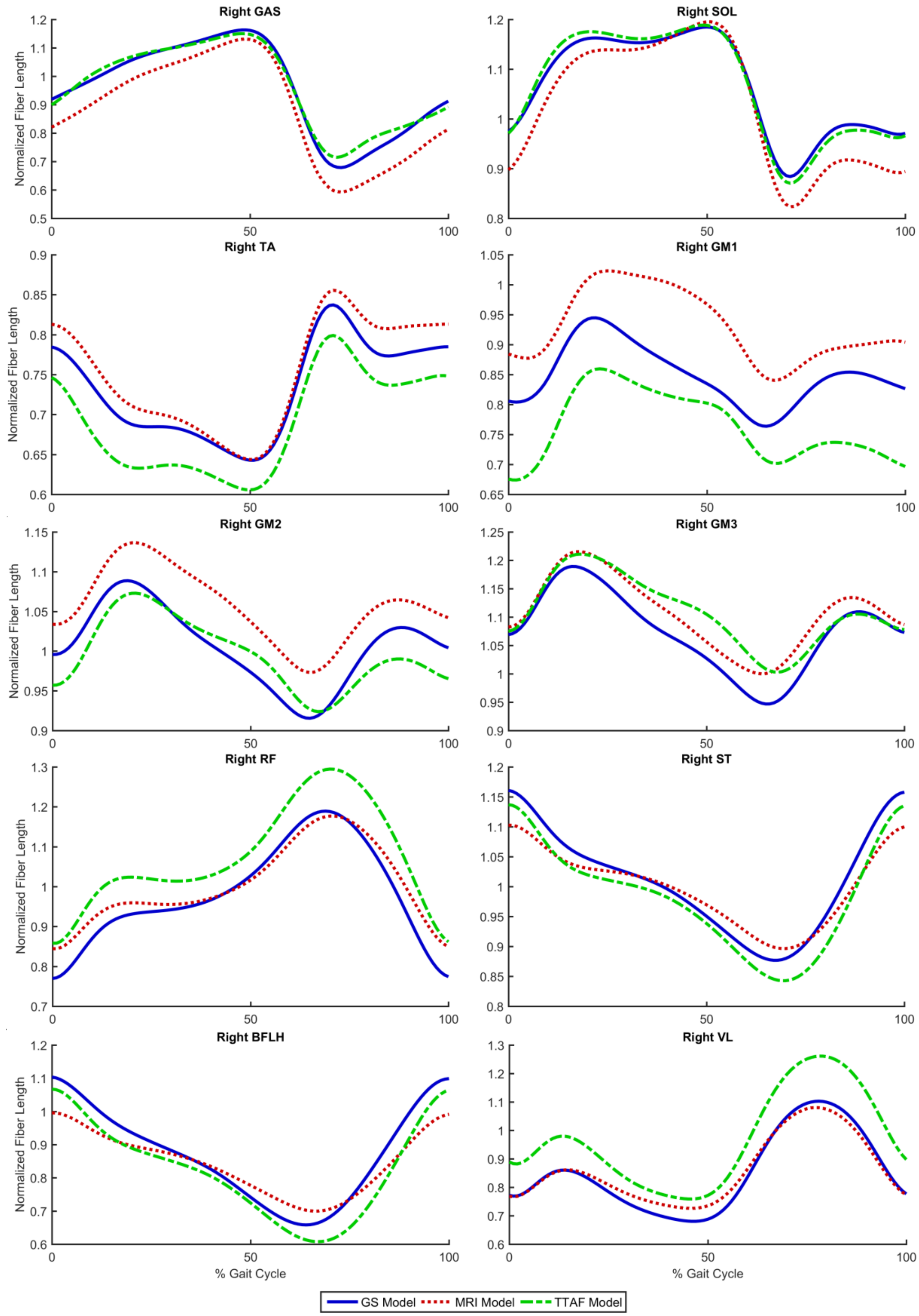

Figure 12: Normalized muscle fiber lengths (NFL) for the right leg

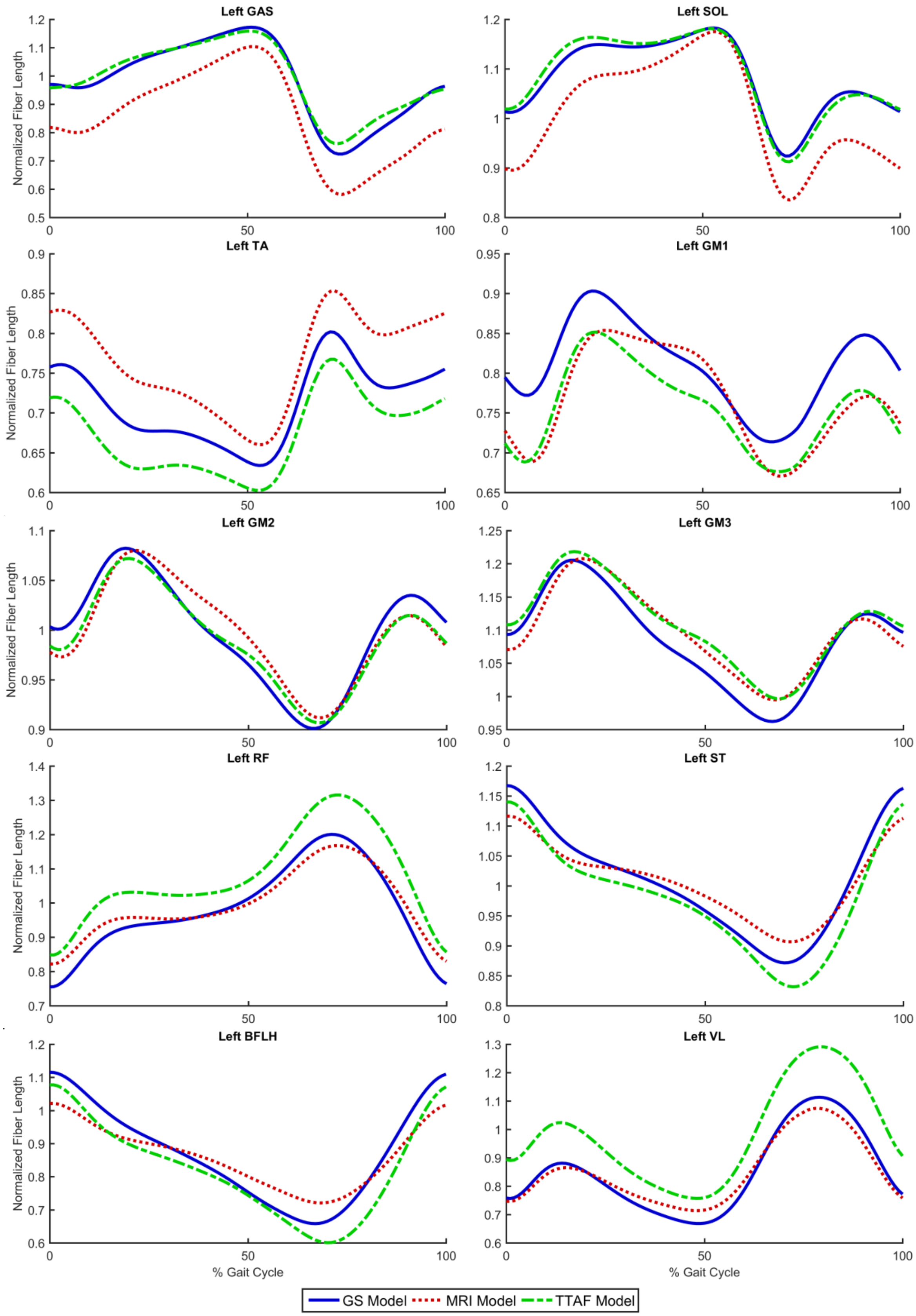

Figure 13: Normalized muscle fiber lengths (NFL) for the left leg

3.6.2 NFL Comparisons with TTAF Model

The TTAF model produced noticeably different results to those from the MRI model, most evident in the VL having the highest differences while GAS had the lowest. In addition, GM1 and RF produced the largest difference in the TTAF model vs the GS model. GM1, GM3, TA, ST, and BFLH were smaller, while RF and VL were larger over the entire gait cycle. GM1-R had slightly slower length change for terminal stance. GM2 was higher from terminal stance until just prior to initial swing (about 70%). Table 12 summarizes these differences and Figure 13 shows that GM1, RF from pre- to mid-swing, and VL from initial to –mid swing were farther from an NFL of 1, but the RF and VL were closer to 1 during the remaining phases.

Table 12: Mean dGT of overall-average NFLs for each phase of gait. Standard deviations range from 0.001 to 0.022.

Stride Phase		0 – 10%	10 – 30%	30 – 50%	50 – 60%	60 – 75%	75 – 87%	87 – 100%
R	GAS	0.012	0.012	0.008	0.014	0.022	0.043	0.015
	SOL	0.010	0.014	0.007	0.004	0.012	0.014	0.008
	TA	0.050	0.054	0.042	0.035	0.037	0.036	0.037
	GM1	0.125	0.091	0.054	0.030	0.067	0.109	0.125
	GM2	0.036	0.015	0.013	0.027	0.012	0.031	0.040
	GM3	0.008	0.029	0.065	0.078	0.051	0.008	0.003
	RF	0.091	0.090	0.063	0.071	0.101	0.125	0.111
	ST	0.025	0.026	0.015	0.015	0.033	0.050	0.036
	BFLH	0.041	0.045	0.022	0.024	0.059	0.093	0.061
	VL	0.114	0.106	0.079	0.101	0.143	0.160	0.147
L	GAS	0.011	0.018	0.007	0.014	0.020	0.043	0.014
	SOL	0.015	0.018	0.004	0.003	0.009	0.015	0.004
	TA	0.046	0.051	0.038	0.031	0.034	0.031	0.038
	GM1	0.082	0.056	0.043	0.031	0.037	0.056	0.073
	GM2	0.020	0.010	0.003	0.013	0.006	0.014	0.020
	GM3	0.012	0.017	0.036	0.049	0.034	0.007	0.006
	RF	0.099	0.099	0.063	0.061	0.101	0.133	0.120
	ST	0.030	0.030	0.015	0.011	0.031	0.054	0.040
	BFLH	0.044	0.049	0.022	0.013	0.053	0.097	0.065
	VL	0.137	0.129	0.093	0.103	0.152	0.179	0.164

3.7 TSL and MIF Comparisons

GS and TTAF models contained the same MIF values because they both used the same scaling method, while differences in TSL were small, with an average of 0.1 ± 0.3 mm. MRI had significantly larger MIF values than the GS model for the RF, VL, and SOL-L, and moderately larger MIFs for GAS-L and GM1-R. On the other hand, BFLH and TA had significantly lower MIFs. MRI models had noticeably shorter TSLs for the GAS-L, SOL-L, TA-L and GM1, but longer lengths for ST, BFLH, RF, and VL. Average parameter values are summarized in Table 13.

Table 13: Average MIF and TSL values for muscles of interest

		MIF [N]					TSL [mm]				
		GS		MRI		GS – MRI	GS		MRI		GS – MRI
		Avg	STDEV	Avg	STDEV		Avg	STDEV	Avg	STDEV	
R	GM1	548	96	650	116	-102	66.81	6.69	53.32	6.29	13.49
	GM2	383	67	455	81	-72	45.11	4.66	36.02	4.27	9.09
	GM3	437	77	519	92	-82	45.29	4.73	37.49	4.38	7.80
	ST	274	48	211	72	64	230.72	30.94	254.11	29.16	-23.38
	BFLH	600	105	294	69	306	292.96	39.91	324.60	38.41	-31.64
	RF	782	137	1140	229	-358	273.90	36.34	292.68	35.95	-18.78
	VL	1252	220	1825	367	-573	139.45	19.15	153.51	19.26	-14.06
	GAS	1043	183	1059	157	-16	362.24	40.16	356.35	30.34	5.89
	SOL	2375	416	2412	359	-37	232.76	26.16	230.47	17.65	2.29
	TA	606	106	359	65	247	205.53	20.43	200.74	18.56	4.78
L	GM1	548	96	634	171	-86	66.66	6.43	53.28	6.84	13.38
	GM2	383	67	444	120	-60	45.01	4.51	35.99	4.61	9.02
	GM3	437	77	506	137	-69	45.17	4.56	37.45	4.84	7.72
	ST	274	48	175	69	99	229.89	28.33	251.27	32.97	-21.38
	BFLH	600	105	306	80	294	291.23	36.37	322.15	44.57	-30.92
	RF	782	137	1080	226	-297	271.35	33.01	292.48	43.06	-21.13
	VL	1252	220	1728	361	-476	138.12	17.37	153.50	23.33	-15.38
	GAS	1043	183	1193	306	-150	367.97	40.73	340.58	24.33	27.39
	SOL	2375	416	2717	696	-342	236.60	26.59	219.92	13.89	16.68
	TA	606	106	306	79	300	208.63	21.08	194.94	16.49	13.69

4.0 Discussion

The main purpose of this thesis was to evaluate how personalizing musculoskeletal models of children with cerebral palsy affects simulation outcomes. To achieve this, 3 models – generic, deformed generic, and MRI-based – were created for each patient, simulated using OpenSim, and assessed with respect to kinematics, kinetics, and muscle activity. In addition, model parameters were also studied to provide more insight into simulation results including MAL, TSL, NFL, and MIF.

Gait kinematics for all 3 model types were found to exhibit patterns commonly found in CP gait [3] [22], but to various degrees. The main differences included increased hip and knee flexion, increased ankle dorsiflexion, increased hip adduction during stance, and delayed knee flexion in terminal stance and early swing. When comparing to healthy gait data it is important to consider differences caused by over-ground vs treadmill walking. With GRAIL, the main differences could include slight decreases in dorsiflexion (about 4°) and increased knee flexion (about 7°) during initial contact [23].

The largest differences between the MRI and GS models were found in the hip and its flexion-extension muscles. Moderate differences were found in the remaining joints and muscles at various times throughout the gait cycle. In TTAF models, on the other hand, variations were more concentrated in the lower leg with low to moderate effects on the hips and muscles of the upper leg. Larger manually measured TT and FA deformation angles did not necessarily lead to greater differences in simulation results for MRI models. This is evident in, for example, CP04 which has the lowest deformation angles, but relatively larger differences in simulation outcomes and model parameters.

EMG signals corresponded well with activations predicted by the models for most muscles. TA agreement varied between patients. EMG for ST indicated slight activation near mid-swing for certain patients and was not always predicted by the models. RF activation predictions had a similar trend to the EMG signal, but were more compressed, occurring from terminal stance to mid-swing rather than over the entire stride. Differences could arise from poor EMG signals, either due to node placement or interference, from EMG filtering, or could indicate model inaccuracies.

Differences in simulation outcomes between models were typically associated with larger differences in TSL, MAL, and MIF. Longer TSL, longer MAL, and lower MIF led to higher muscle activations. In events where differences in a muscle's parameters had varying effects on activation (eg. longer TSL, but shorter MAL), TSL would generally take precedent. These findings are in line with several sensitivity studies such as Carbone et al. [6] and Ackland et al. [7]. Exceptions to this were found in the GAS muscles during pre-swing and toe-off, in TA during swing, and in VL during mid-stance.

When considered along with the SOL muscles, GAS experienced more TSL shortening, SOL had larger MIF increases, and both had longer MAL (common tendon). However, the GAS was found to operate about 0.08 – 0.1 closer to its optimal muscle fiber length in the MRI models, whereas operating lengths in the GS and TTAF models were similar between the 2 muscles. This could indicate that activation of the GAS was more efficient than the SOL in the MRI models during the pre-swing phase. Xiao & Higginson [24] showed plantarflexors had larger sensitivities to TSL and optimal muscle fiber length, with the ability to affect other muscles about the ankle (plantar- and dorsi-flexors) and knee muscles. Meanwhile, VL saw the largest increases in MIF between MRI and GS models: 573 N higher in the right leg and 476 N higher in the left leg.

Hip flexor contracture and spasticity combined with weak hip extensors are often the cause of increased hip flexion in CP [3]. This is reflected in the MRI model's ST and BFLH muscles which show larger activity from initial contact until terminal pre-swing as they attempt to extend the hip. Shorter MAL and longer TSL values for the hamstrings and RF contribute to the higher activations, while MIF values indicate weaker BFLH and ST but stronger RF. RF saw activation begin in mid-stance and carry into terminal swing, with MRI model exceeding the GS at about 40% through the gait cycle.

TTAF and GS models experienced slightly more rotation about the hip, reflected in the higher moments and activations of the GM1 and GM3 muscles from mid to terminal stance. These models also have longer TSL values and lower MIF compared to the MRI models. The right GM1 operates closer to its optimal length in the MRI model, but all remaining GM NFL values are further from 1 or similar to GS muscles. Hip adduction was higher for the MRI models from mid-swing until mid-stance and is reflected in the higher moments, but not in the activation of GM2. GM2 saw lower activations in the MRI model corresponding to shorter TSL and MAL, and larger MIF. Although not studied in this thesis, OpenSim results did show higher activations for other hip abductors such as the gluteus maximus in the MRI models. Regarding the muscles acting on the hip, work by Carbone et al. [9] [6] indicates that MAL and TSL changes applied to individual prime movers or hip stabilizers had the potential to noticeably affect other muscles. Thus, future research should include more hip adductors, abductors, and rotators for a better understanding on the interactions between muscles. Variations in hip muscle moment arms between model types correspond to findings made by Scheys et al. [24] [25] who studied similar comparisons, but with larger femoral anteversion deformations, and found larger variations in moment arms at the hip in MRI-based models.

Increased knee flexion in the MRI models can also be due to the higher hamstring activations mentioned earlier and to lower VL activities in mid-stance. Knees in all models also experience slightly delayed flexion in swing, often caused by RF over-activity in late stance or early swing [22] which is especially evident in simulation outcomes of the left leg. Increased dorsiflexion of all models coincide with larger moments, particularly in mid-stance, and higher TA activity throughout the stride. Lower dorsiflexion (larger plantarflexion) in the MRI models in swing and loading response corresponds to the higher GAS activity beginning in pre-swing. The largest differences in subtalar angles were found in the TTAF models which exhibited more inversion. GAS MAL for TTAF models were found to be in the opposite direction compared to SOL, allowing the muscle to aid in inversion. Subtalar angle was similar between GS and MRI models, except in the right leg from terminal stance until pre-swing, where the MRI model experienced more inversion due to higher TA activity.

Results for the TTAF models were generally consistent with GS outcomes across all simulation outcomes and parameters in terms of the trends they exhibited over the gait cycle as can be seen by the shape of the plots included in this report. The largest differences appear in the moment arm lengths and moments of the subtalar joints and are mainly reflected in the lower leg muscle activations during mid-stance.

Limitations of the study include the small sample size and that patients generally had low bone deformations (average FA deformation –from healthy FA – was 4.58° ± 3.96°; average TA was 10.83° ± 7.02°) which could be subject to error from manual measurement [17] [18] and from the fact that the rotation algorithms are estimations [19] [20] [21]. All models also used knees with 1 degree of freedom , excluding knee translation.

The MRI models had slightly larger scaling and kinematic errors, which could have been caused by the virtual MRI marker set. The virtual markers for GS models were obtained using boney landmarks on the

Gait 2392 model, whereas MRI markers were obtained using boney landmarks in MR images. Additionally, torso markers were not identified in the images, leading to manual placement on the models once loaded into OpenSim. CP05, while still following general trends, exhibited vibration in joint moments most evident in the subtalar and ankle joints. One possible cause could be vibration in the force plate data. Filtering techniques may be able to smoothen the data, making it more suitable for simulation.

A software glitch associated with the Thelen 2003 Muscle Model used by the default Gait 2392 model was found to frequently cause sporadic muscle-tendon length activity, leading to the use of the Millard 2012 Equilibrium Muscle Model instead. The Static Optimization tool took an abnormally longer time to process the data. Appending muscle actuation, commonly employed in healthy gait simulations [27], increased the speed indicating that the models may be under-actuated at times. The work in this report did not use additional muscle actuators as they are not physiologically realistic. Comparisons with EMG indicate good qualitative relation to the activations predicted by OpenSim, however magnitudes may be affected.

5.0 Conclusions

Generic, deformed generic, and MRI-based models were found to exhibit similar kinematic and kinetic behaviors throughout the gait cycle, but varied in magnitude. These variations corresponded to differences in muscle activations as well as muscle-model and geometric parameters. Tendon slack length was the main factor for most muscle activity differences, followed by moment arm lengths, and normalized fiber lengths, which were found to impact the plantarflexors. MRI model outcomes mainly differed from GS models about the hip, specifically hamstrings and quadriceps, and also experienced moderate differences in the lower leg and foot. Meanwhile, TTAF model outcomes mainly differed from the GS models around the subtalar joint. Larger bone deformation angles did not lead to greater differences in simulation results for MRI models, but did in TTAF models. As a "partially personalized" model, simulation outcomes for TTAF models did not lie between those of GS and MRI. These findings suggest that the deformations alone do not account for other influential factors. The manual measurement methods used to obtain the angles also entail potential errors, therefore measurement from medical images could be a more accurate representation of the actual deformity. While the musculoskeletal models are valuable in providing insight into muscle interactions and their contributing factors, they lack accuracy and validation required to make them more reliable in intervention planning.

Literature suggests that changes to hip stabilizers and prime movers have the potential to affect other muscles more than them perturbed muscles themselves. Thus, it is recommended for future studies to incorporate pelvis movement and more muscles into analysis, such as the psoas, gluteus maximus, hip rotators, and muscles involved in subtalar inversion and eversion. Exploration of filtering techniques can also be useful in comparisons with EMG for validation and in smoothening data for use in simulation. It is also recommended to analyze more patients with cerebral palsy with varying levels of bone deformity to add to the existing pool of knowledge. Finally, creating models for children with CP before and after intervention and comparing simulation results between them could provide additional insight and help in validation.

Acknowledgements

I would like to thank Thomas Geijtenbeek and Marjolein van der Krogt who guided me throughout my literature study, internship, and thesis. Their insight into problems I faced along the way and suggestions on how to approach various tasks helped immensely. I would also like to that family and friends, both those from home and those met during my time in the Netherlands, for their continuous support. Organizing Skype calls back home was not always easy with the time difference, but always made my weeks better.

References

[1] M. H. Schwartz, A. Rozumalski and J. P. Trost, "The effect of walking speed on the gait of typically developing children," *Journal of Biomechanics,* vol. 41, pp. 1639-1650, 2008.

[2] M. G. Pandy and T. P. Andriacchi, "Muscle and Joint Function in Human Locomotion," *Annual Review of Biomedical Engineering,* vol. 12, pp. 401-433, 2010.

[3] F. M. Chang, J. T. Rhodes, K. M. Flynn and J. J. Carollo, "The role of gait analysis in treating gait abnormalities in Cerebral Palsy," *Orthopedic Clinics of North America,* vol. 41, pp. 489-506, 2010.

[4] S. L. Delp, F. C. Anderson, A. S. Arnold, P. Loan, A. Habib, C. T. John, E. Guendelman and D. G. Thelen, "OpenSim: Open-Source Software to Create and Analyze Dynamic Simulations of Movement," *IEEE Transactions on Biomedical Engineering,* vol. 54, no. 11, pp. 1940-1950, 2007.

[5] E. M. Arnold, S. R. Ward, R. L. Lieber and S. L. Delp, "A Model of the Lower Limb for Analysis of Human Movement," *Annals of Biomedical Engineering,* vol. 38, no. 2, pp. 269-279, 2010.

[6] V. Carbone, M. M. van der Krogt, H. F. J. M. Koopman and N. Verdonschot, "Sensitivity of subject specific models to hill muscle-tendon model parameters in simulations of gait," *Journal of Biomechanics,* vol. 49, no. 9, pp. 1953-1960, 2016.

[7] D. C. Ackland, Y.-C. Lin and M. G. Pandy, "Sensitivity of model predictions of muscle function to changes in moment arms and muscle–tendon properties- A Monte-Carlo analysis," *Journal of Biomechanics,* vol. 45, pp. 1463-1471, 2012.

[8] F. De Groote, A. Van Campen, I. Jonkers and J. De Schutter, "Sensitivity of dynamic simulations of gait and dynamometer experiments to Hill muscle model parameters of knee flexors and extensors," *Journal of Biomechanics,* vol. 43, pp. 1876-1883, 2010.

[9] V. Carbone, M. M. van der Krogt, H. F. J. M. Koopman and N. Verdonschot, "Sensitivity of subject-specific models to errors in musculoskeletal geometry," *Journal of Biomechanics,* vol. 45, no. 14, pp. 2476-2480, 2012.

[10] L. Bosmans, G. Valente, M. Wesseling, A. V. Campen, F. De Groote, J. De Schutter and I. Jonkers, "Sensitivity of predicted muscle forces during gait to anatomical variability in musculotendon geometry," *Journal of Biomechanics,* vol. 48, no. 10, pp. 2116-2123, 2015.

[11] M. D. Klein Horsman, H. F. J. M. Koopman, F. C. T. van der Helm, L. P. Prosé and H. E. J. Veeger, "Morphological muscle and joint parameters for musculoskeletal modelling of the lower extremity," *Clinical Biomechanics,* vol. 22, pp. 239-247, 2007.

[12] A. S. Arnold, S. Salinas, D. J. Asakawa and S. L. Delp, "Accuracy of Muscle Moment Arms Estimated from MRI-Based Musculoskeletal Models of the Lower Extremity," *Computer Aided Surgery,* vol. 5, pp. 108-119, 2000.

[13] L. Scheys, I. Jonkers, D. Loeckx, F. Maes, A. Spaepen and P. Suetens, "Image Based Musculoskeletal Modeling Allows Personalized Biomechanical Analysis of Gait," *Biomedical Simulation,* vol. 4071, pp. 58-66, 2006.

[14] L. Scheys, D. Loeckx, A. Spaepen, P. Suetens and I. Jonkers, "Atlas-based non-rigid image registration to automatically define line-of-action muscle models: A validation study," *Journal of Biomechanics,* vol. 42, pp. 565-572, 2009.

[15] P. Pellikaan, M. M. van der Krogt, V. Carbone, R. Fluit, L. M. Vigneron, J. Van Deun, N. Verdonschot and H. F. J. M. Koopman, "Evaluation of a morphing based method to estimate muscle attachment sites of the lower extremity," *Journal of Biomechanics,* vol. 47, pp. 1144-1150, 2014.

[16] U. G. Narayanan, "Management of Children With Ambulatory Cerebral Palsy: An Evidence-based Review," *Journal of Pediatric Orthopaedics,* vol. 32, pp. 172-181, 2012.

[17] R. B. Souza and C. M. Powers, "Concurrent Criterion-Related Validity and Reliability of a Clinical Test to Measure Femoral Anteversion," *Journal of Orthopaedic & Sports Physical Therapy,* vol. 39, no. 8, 2009.

[18] S. H. Lee, C. Y. Chung, M. S. Park, I. H. Choi and T.-J. Cho, "Tibial Torsion in Cerebral Palsy," *Clinical Orthopaedics and Related Research,* vol. 467, pp. 2098-2104, 2009.

[19] A. S. Arnold, S. A. Blemker and S. L. Delp, "Evaluation of a deformable musculoskeletal model for estimating muscle-tendon lengths during crouch gait," *Annals of biomedical engineering,* vol. 29, no. 3, pp. 263-274, 2001.

[20] A. S. Arnold and S. L. Delp, "Rotational moment arms of the medial hamstrings and adductors vary with femoral geometry and limb position: implications for the treatment of internally rotated gait," *Journal of Biomechanics,* vol. 34, no. 4, pp. 437-447, 2001.

[21] J. Hicks, A. Arnold, F. Anderson, M. Schwartz and S. Delp, "The effect of excessive tibial torsion on the capacity of muscles to extend the hip and knee during single-limb stance," *Gait & Posture,* vol. 26, no. 4, pp. 546-552, 2007.

[22] S. Armand, G. Decoulon and A. Bonnefoy-Mazure, "Gait analysis of children with cerebral palsy," *Effort Open Reviews,* vol. 1, pp. 448-460, 2016.

[23] M. M. van der Krogt, L. H. Sloot and J. Harlaar, "Overground versus self-paced treadmill walking in a virtual environment in children with cerebral palsy," *Gait & Posture,* vol. 4, pp. 587-593, 2014.

[24] M. Xiao and J. Higginson, "Sensitivity of estimated muscle force in forward simulation of normal walking," *Journal of Applied Biomechanics,* vol. 26, no. 2, pp. 142-149, 2010.

[25] L. Scheys, A. Van Campenhout, A. Spaepen, P. Suetens and I. Jonkers, "Personalized MR-based musculoskeletal models compared to rescaled generic models in the presence of increased femoral anteversion: Effect on hip moment arm lengths," *Gait & Posture,* vol. 28, pp. 358-365, 2008.

[26] L. Scheys, K. Desloovere, P. Suetens and I. Jonkers, "Level of subject-specific detail in musculoskeletal models affects hip moment arm length calculation during gait in pediatric subjects with increased femoral anteversion," *Journal of Biomechanics,* vol. 44, pp. 1346-1353, 2011.

[27] J. L. Hicks, T. K. Uchida, A. Seth, A. Rajagopal and S. L. Delp, "Is My Model Good Enough? Best Practices for Verification and Validation of Musculoskeletal Models and Simulations of Movement," *Journal of Biomechanical Engineering,* vol. 137, 2015.

APPENDIX – OpenSim Markers & Scaling Marker Pairs

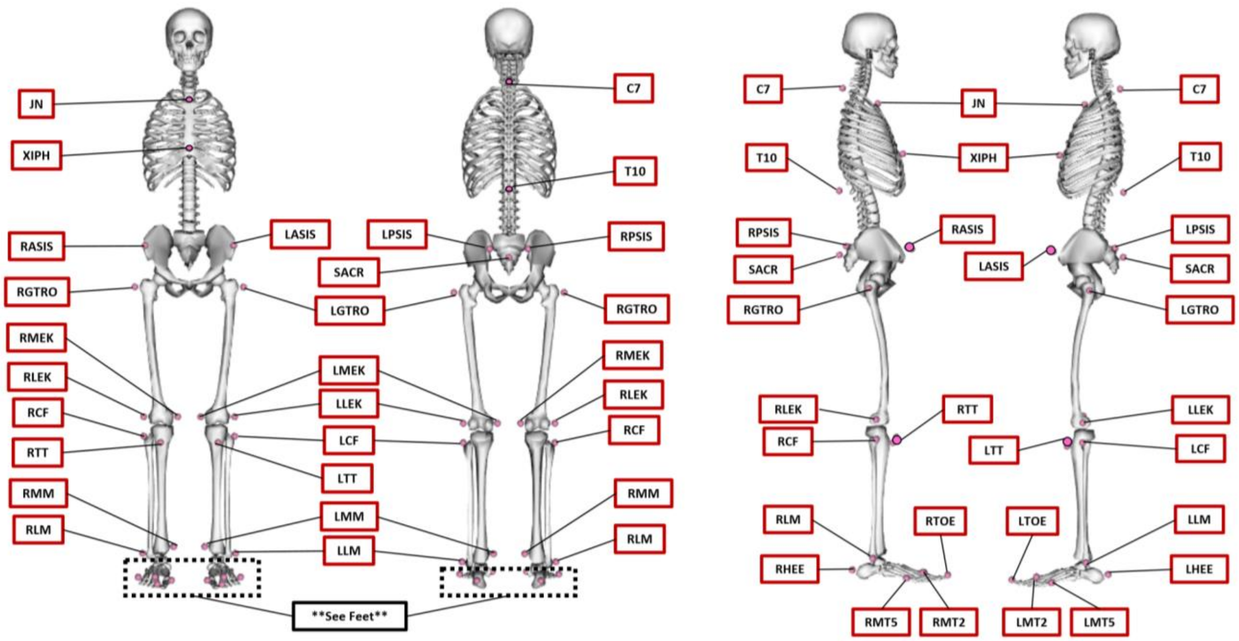

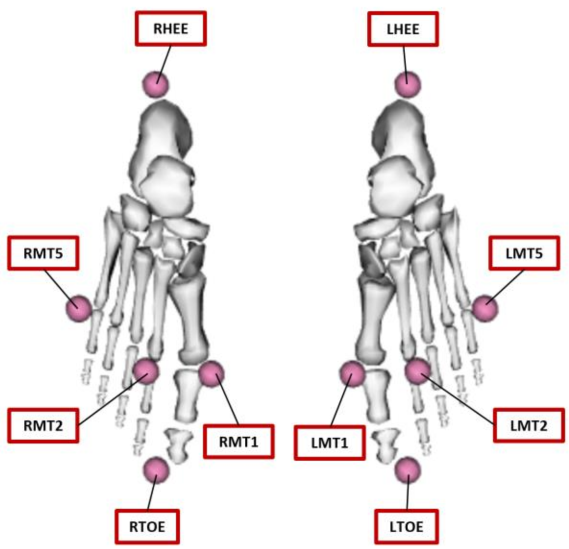

Alternate Names
STRN – JN
XIPH – XYPH
RCF –RFH
LCF - LFH

All markers present in the figures above are present in both GS and TTAF models.
MRI models use a smaller marker set based on anatomical bony landmarks identified in the MR images:

LASIS	LLM	LMT2
RASIS	RLM	RMT2
LPSIS	LMM	LMT5
RPSIS	RMM	RMT5
LLEK	LHEE	LGTRO
RLEK	RHEE	RGTRO
LMEK	LTOE	LFH
RMEK	RTOE	RFH

VUmc Marker Pairs

Segment (direction)	Scaling Factor			
Torso (SI)	RASIS-C7	LASIS-C7	RPSIS-C7	LPSIS-C7
Torso (AP)	T10-STRN	C7-STRN		
Torso (ML)	SACR-LASIS	SACR-RASIS		
Pelvis (SI)	RASIS-LASIS	LPSIS-LASIS		
Pelvis (AP)	LASIS-LPSIS	RASIS-RPSIS		
Pelvis (ML)	RASIS-LASIS			
Thigh_R	RGTRO-RLEK	RASIS-RLEK		
Thigh_L	LGTRO-LLEK	LASIS-LLEK		
Shank_R	RCF-RLM	RTT-RMM		
Shank_L	LCF-LLM	LTT-LMM		
Foot_R	RMT5-RMT1	RHEE-RTOE		
Foot_L	LMT5-LMT1	LHEE-LTOE		

*If no direction is provided, a single factor is used to scale in all directions (i.e. uniform scaling)
** '_R' and '_L' signify right and left, respectively

If SACR was not available in experimental data:

Pelvis (SI)	RASIS-LASIS	LPSIS-LASIS	RPSIS-RASIS

APPENDIX – Scaling and Kinematic Errors

SCALING ERRORS

GS Models				
Subject	**Total Squared Error**	**RMS**	**Maximum**	**Marker**
CP02	0.0101	0.0175	0.0405	RPSIS
CP03	0.0075	0.0151	0.0303	LGTRO
CP04	0.0150	0.0216	0.0612	XYPH
CP05	0.0134	0.0202	0.0373	XYPH
CP07	0.0127	0.0196	0.0358	LGTRO
CP08	0.0120	0.0197	0.0331	C7
CP09	0.0149	0.0213	0.0406	LMEK
TTAF Models				
Subject	**Total Squared Error**	**RMS**	**Maximum**	**Marker**
CP02	0.0101	0.0175	0.0399	RPSIS
CP03	0.0078	0.0153	0.0284	RMEK
CP04	0.0148	0.0215	0.0606	XYPH
CP05	0.0133	0.0201	0.0367	XYPH
CP07				
CP08	0.0124	0.0200	0.0338	C7
CP09	0.0158	0.0219	0.0405	LMEK
MRI Models				
Subject	**Total Squared Error**	**RMS**	**Maximum**	**Marker**
CP02	0.0316	0.0336	0.0598	LPSIS
CP03	0.0219	0.0280	0.0543	RGTRO
CP04	0.0433	0.0400	0.0795	RGTRO
CP05	0.0453	0.0402	0.0741	RGTRO
CP07	0.0293	0.0323	0.0510	LPSIS
CP08	0.0345	0.0364	0.0615	RPSIS
CP09	0.0240	0.0293	0.0508	RGTRO

Total squared errors presented in [m^2]
RMS and maximum errors presented in [m]

KINEMATIC ERRORS

Subject	**Total Squared Error [m^2]**			**RMS Error [m]**			**Maximum Error [m]**		
	GS	**MRI**	**TTAF**	**GS**	**MRI**	**TTAF**	**GS**	**MRI**	**TTAF**
CP02	0.0052	0.0050	0.0052	0.0136	0.0147	0.0136	0.0293	0.0305	0.0304
CP03	0.0025	0.0029	0.0031	0.0095	0.0109	0.0105	0.0200	0.0208	0.0213
CP04	0.0029	0.0066	0.0034	0.0103	0.0167	0.0112	0.0231	0.0457	0.0248
CP05	0.0061	0.0066	0.0066	0.0145	0.0161	0.0151	0.0387	0.0386	0.0394
CP07	0.0019	0.0022		0.0083	0.0097		0.0174	0.0199	
CP08	0.0048	0.0063	0.0048	0.0128	0.0162	0.0129	0.0311	0.0361	0.0308
CP09	0.0021	0.0023	0.0020	0.0089	0.0102	0.0088	0.0239	0.0228	0.0239
Average	0.0036	0.0046	0.0042	0.0111	0.0135	0.0120	0.0262	0.0306	0.0285

APPENDIX – Standard Deviations for Muscle Activations

STDEV dGM		0 to 10	10 to 30	30 to 50	50 to 60	60 to 75	75 to 87	87 to 100
R	GAS	0.0100	0.0224	0.0105	0.0415	0.0479	0.0016	0.0023
	SOL	0.0305	0.0263	0.0167	0.0374	0.0054	0.0001	0.0002
	TA	0.0339	0.0087	0.0105	0.0231	0.0187	0.0087	0.0035
	GM1	0.0182	0.0263	0.0088	0.0329	0.0074	0.0032	0.0067
	GM2	0.0188	0.0353	0.0059	0.0287	0.0033	0.0017	0.0021
	GM3	0.0220	0.0391	0.0062	0.0220	0.0118	0.0035	0.0071
	RF	0.0088	0.0202	0.0326	0.0264	0.0230	0.0103	0.0065
	ST	0.0268	0.0706	0.0147	0.0295	0.0046	0.0085	0.0528
	BFLH	0.0297	0.0519	0.0164	0.0259	0.0034	0.0103	0.0464
	VL	0.0248	0.0342	0.0046	0.0065	0.0032	0.0013	0.0007
L	MGAS	0.0177	0.0288	0.0114	0.0478	0.0430	0.0027	0.0030
	SOL	0.0227	0.0338	0.0178	0.0302	0.0163	0.0017	0.0002
	TA	0.0500	0.0242	0.0060	0.0114	0.0250	0.0150	0.0106
	GM1	0.0156	0.0307	0.0116	0.0412	0.0095	0.0052	0.0032
	GM2	0.0087	0.0227	0.0096	0.0203	0.0072	0.0023	0.0061
	GM3	0.0233	0.0207	0.0135	0.0160	0.0141	0.0026	0.0042
	RF	0.0161	0.0194	0.0130	0.0145	0.0156	0.0126	0.0107
	ST	0.0667	0.0895	0.0184	0.0141	0.0033	0.0020	0.0293
	BFLH	0.0573	0.0704	0.0223	0.0082	0.0029	0.0042	0.0365
	VL	0.0264	0.0356	0.0058	0.0094	0.0011	0.0012	0.0003

	STDEV dGT	0 to 10	10 to 30	30 to 50	50 to 60	60 to 75	75 to 87	87 to 100
R	GAS	0.0143	0.0205	0.0122	0.0137	0.0048	0.0008	0.0026
	SOL	0.0036	0.0072	0.0055	0.0132	0.0049	0.0001	0.0002
	TA	0.0180	0.0101	0.0067	0.0084	0.0035	0.0033	0.0038
	GM1	0.0019	0.0136	0.0047	0.0055	0.0038	0.0015	0.0008
	GM2	0.0052	0.0164	0.0045	0.0059	0.0029	0.0020	0.0016
	GM3	0.0168	0.0141	0.0112	0.0117	0.0044	0.0016	0.0025
	RF	0.0064	0.0129	0.0134	0.0017	0.0086	0.0029	0.0023
	ST	0.0126	0.0119	0.0038	0.0058	0.0020	0.0008	0.0042
	BFLH	0.0167	0.0089	0.0057	0.0059	0.0014	0.0007	0.0035
	VL	0.0102	0.0102	0.0041	0.0008	0.0006	0.0010	0.0005
L	MGAS	0.0074	0.0107	0.0114	0.0040	0.0048	0.0010	0.0040
	SOL	0.0031	0.0018	0.0029	0.0169	0.0132	0.0001	0.0003
	TA	0.0254	0.0173	0.0107	0.0170	0.0031	0.0026	0.0046
	GM1	0.0007	0.0039	0.0024	0.0030	0.0036	0.0006	0.0007
	GM2	0.0025	0.0032	0.0036	0.0051	0.0038	0.0040	0.0021
	GM3	0.0016	0.0091	0.0039	0.0070	0.0046	0.0067	0.0096
	RF	0.0081	0.0070	0.0053	0.0133	0.0107	0.0049	0.0041
	ST	0.0074	0.0057	0.0023	0.0029	0.0020	0.0009	0.0028
	BFLH	0.0105	0.0087	0.0038	0.0031	0.0012	0.0009	0.0021
	VL	0.0054	0.0055	0.0029	0.0014	0.0007	0.0005	0.0013

APPENDIX – Normalized Fiber Length Distances from 1

Distance of normalized muscles fiber lengths (NFL) from 1. Negative values indicate below 1 while positive value indicate above 1.

med_gas_r	0 to 10	10 to 30	30 to 50	50 to 60	60 to 75	75 to 87	87 to 100
GS	-0.05	0.05	0.14	0.10	-0.22	-0.26	-0.15
MRI	-0.14	-0.02	0.09	0.06	-0.30	-0.36	-0.25
TTAF	-0.05	0.06	0.13	0.09	-0.20	-0.22	-0.15
soleus_r							
GS	0.03	0.15	0.17	0.15	-0.05	-0.04	-0.02
MRI	-0.04	0.12	0.16	0.16	-0.10	-0.11	-0.10
TTAF	0.04	0.16	0.17	0.15	-0.06	-0.05	-0.03
tib_ant_r							
GS	-0.23	-0.30	-0.34	-0.34	-0.20	-0.21	-0.22
MRI	-0.20	-0.28	-0.33	-0.33	-0.19	-0.18	-0.19
TTAF	-0.28	-0.36	-0.38	-0.37	-0.24	-0.25	-0.26
glut_med1_r							
GS	-0.18	-0.08	-0.13	-0.19	-0.22	-0.16	-0.16
MRI	-0.12	-0.01	0.00	-0.07	-0.14	-0.11	-0.10
TTAF	-0.31	-0.17	-0.18	-0.22	-0.29	-0.27	-0.28
glut_med2_r							
GS	0.01	0.07	0.01	-0.05	-0.07	0.01	0.02
MRI	0.05	0.12	0.08	0.01	-0.01	0.05	0.06
TTAF	-0.02	0.06	0.02	-0.02	-0.07	-0.02	-0.02
glut_med3_r							
GS	0.10	0.17	0.07	0.00	-0.03	0.07	0.09
MRI	0.12	0.20	0.11	0.03	0.02	0.11	0.11
TTAF	0.11	0.20	0.14	0.07	0.02	0.08	0.09
rect_fem_r							
GS	-0.19	-0.08	-0.03	0.08	0.17	0.08	-0.14
MRI	-0.13	-0.05	-0.02	0.06	0.16	0.11	-0.07
TTAF	-0.10	0.01	0.04	0.15	0.27	0.21	-0.03
semiten_r							
GS	0.13	0.05	-0.01	-0.08	-0.11	-0.04	0.11
MRI	0.09	0.03	0.00	-0.05	-0.09	-0.05	0.06
TTAF	0.11	0.03	-0.02	-0.09	-0.15	-0.09	0.07
bifemlh_r							
GS	0.07	-0.06	-0.18	-0.30	-0.32	-0.16	0.04
MRI	-0.02	-0.10	-0.17	-0.25	-0.29	-0.20	-0.06
TTAF	0.03	-0.10	-0.20	-0.32	-0.38	-0.26	-0.02
vas_lat_r							
GS	-0.20	-0.18	-0.30	-0.25	-0.01	0.08	-0.10
MRI	-0.20	-0.17	-0.26	-0.21	-0.01	0.06	-0.12
TTAF	-0.09	-0.08	-0.22	-0.15	0.13	0.24	0.04

med_gas_l	0 to 10	10 to 30	30 to 50	50 to 60	60 to 75	75 to 87	87 to 100
GS	-0.04	0.03	0.13	0.14	-0.16	-0.22	-0.09
MRI	-0.19	-0.10	0.04	0.07	-0.28	-0.36	-0.24
TTAF	-0.03	0.05	0.13	0.13	-0.14	-0.17	-0.08
soleus_l							
GS	0.03	0.13	0.16	0.17	-0.01	0.01	0.04
MRI	-0.08	0.06	0.12	0.16	-0.07	-0.08	-0.07
TTAF	0.05	0.15	0.16	0.16	-0.02	0.00	0.04
tib_ant_l							
GS	-0.25	-0.31	-0.34	-0.36	-0.24	-0.25	-0.26
MRI	-0.18	-0.25	-0.30	-0.33	-0.20	-0.19	-0.19
TTAF	-0.29	-0.36	-0.38	-0.39	-0.27	-0.28	-0.30
glut_med1_l							
GS	-0.22	-0.13	-0.16	-0.23	-0.28	-0.21	-0.17
MRI	-0.30	-0.19	-0.16	-0.22	-0.31	-0.28	-0.24
TTAF	-0.30	-0.18	-0.21	-0.26	-0.31	-0.27	-0.24
glut_med2_l							
GS	0.01	0.07	0.00	-0.06	-0.09	-0.01	0.03
MRI	-0.02	0.06	0.03	-0.03	-0.08	-0.03	0.00
TTAF	-0.01	0.06	0.00	-0.05	-0.08	-0.03	0.01
glut_med3_l							
GS	0.12	0.18	0.08	0.01	-0.03	0.06	0.11
MRI	0.10	0.19	0.12	0.04	0.01	0.07	0.10
TTAF	0.13	0.20	0.12	0.06	0.01	0.07	0.12
rect_fem_l							
GS	-0.20	-0.08	-0.03	0.06	0.17	0.11	-0.13
MRI	-0.14	-0.05	-0.03	0.03	0.14	0.12	-0.07
TTAF	-0.10	0.02	0.03	0.12	0.27	0.25	-0.01
semiten_l							
GS	0.14	0.06	-0.01	-0.06	-0.12	-0.06	0.10
MRI	0.10	0.04	0.01	-0.04	-0.08	-0.05	0.06
TTAF	0.11	0.03	-0.02	-0.08	-0.15	-0.11	0.06
bifemlh_l							
GS	0.09	-0.05	-0.17	-0.28	-0.33	-0.20	0.03
MRI	0.00	-0.08	-0.15	-0.23	-0.27	-0.20	-0.05
TTAF	0.04	-0.09	-0.20	-0.30	-0.38	-0.29	-0.04
vas_lat_l							
GS	-0.20	-0.16	-0.30	-0.29	-0.04	0.10	-0.09
MRI	-0.22	-0.16	-0.26	-0.25	-0.04	0.06	-0.12
TTAF	-0.07	-0.03	-0.21	-0.19	0.11	0.27	0.07